New Folder Name _Birefringence and Refractive Index_

Birefringence and Refractive Index Inhomogeneity in Fused Silica Test Masses

Michael Burka

9 February 1990

Abstract

Two pieces of high grade fused silica were tested in a Fizeau interferometer to determine the magnitude and spatial distribution of refractive index inhomogeneity and birefringence. The data was used as input to a Monte Carlo simulation of LIGO-scale mirrors, and it is shown that if index inhomogeneity and birefringence are limiting factors, then interferometer contrast will lie between .989 and .999.

1 Introduction

Refractive index inhomogeneity and residual birefringence in thick glass blanks are a result of residual stresses left from the annealing process.[1] The goal of this experiment was to measure the magnitude and spatial characteristics of the refractive index inhomogeneity and residual birefringence of two pieces of fused silica. The technique was to pass a nearly flat wavefront through each piece, and to measure the phase variation of the resultant wavefront interferometrically.

2 Test pieces

Two blanks of Corning 7940 grade 0A fused silica were tested. This is Corning's finest grade of fused silica. It is produced via a vapor deposition process. Corning's specifications $\Delta n = 1.0 \times 10^{-6}$ for refractive index inhomogeneity and 5 nm/cm for the intrinsic birefringence. Both samples were

---

[1] M. Burka, *On the LIGO Receiver Mirrors*, unpublished LIGO memo, and references therein.

annealed a second time by Corning to reduce the intrinsic birefringence to 1 nm/cm.

One piece was 4.5 inches in diameter by 1.5 inches thick, the other was 4.0 inches in diameter by 3.5 inches thick. The latter piece had a one inch diameter hole drilled through its center for reasons unrelated to this experiment. Both surfaces of each blank were polished flat to a surface quality of $\lambda/50$ peak-to-valley ($\lambda=6328$ angstroms). The polishing was done by Zygo Corporation.

3 Procedure

The blanks were tested with a Zygo Mark IV Fizeau interferometer.[2,3] A schematic of the interferometer is shown in Figure 1. A spatially filtered Helium-Neon laser beam ($\lambda = 6328$ Å) is linearly polarized with a polarizing beamsplitter. The orthogonal component is not used. After reflection from a folding mirror the polarization is changed to circular with a $\lambda/4$ plate. For our linear polarization measurements it was converted back to linear polarization with a polarizer inserted into the intererometer by hand. Some light is reflected from the back of the transmission element, the rest propagates through the test piece to a reflector. The reflectance of the reflector is equal to that of the transmission element (both are uncoated, and reflect about 4% of the incident light), and the light which is reflected propagates through the test piece a second time and recombines with the light reflected from the transmission element. The test piece is tilted slightly so that light reflected from its surfaces does not interfere.

The interference pattern is imaged onto a 244×388 pixel CID array. A neutral density filter served to keep the pattern intensity within the dynamic range of the array, and a zoom lens allowed variable magnification. The optical path shown at the far left of Figure 1, with the alignment reticle, was used only to align the optical components, and did not play a role in the measurements. In the measurement process, the position of the transmission element is changed in quarter-wavelength steps. The resultant interference patterns can be manipulated to yield an array of optical path differences.[4]

Thirty "shots" were recorded. Table 1 is a listing of them. The shots were taken with circularly polarized light, except where a linear polarizer

[2]Bruce E. Truax, *Surface Characterization and Testing*, SPIE vol. 680, 1986.

[3]Moshe Schaham, *Precision Optical Wavefront Measurement*, SPIE vol. 306, 1981.

[4]ibid.

orientation is described.

Shot	Piece	Description
WFA	3.5"	Full aperture - no polarizer
WFB	3.5"	Full aperture - rotated 180° about vertical
WFC	3.5"	Full aperture - rotated approx. -135° about axis
WFD	3.5"	Polarizer at 0° (vertical)
WFE	3.5"	Polarizer at 45°
WFF	3.5"	Polarizer at 90°
WFG	3.5"	Polarizer at 90°
WFH	3.5"	Polarizer at 135°
WFI	3.5"	Polarizer at 157.5°
WFJ	3.5"	Polarizer at 180°
WFK	3.5"	No polarizer
WGD	3.5"	No polarizer - 6X zoom
WFN	1.5"	Full aperture - no polarizer
WFO	1.5"	Polarizer at 0°
WFP	1.5"	Polarizer at 45°
WFQ	1.5"	Polarizer at 90°
WFR	1.5"	Polarizer at 135°
WFS	1.5"	Polarizer at 157.5°
WFT	1.5"	Polarizer at 180°
WFU	1.5"	No polarizer - rotated 180° about vertical
WFV	1.5"	No polarizer - 6X zoom
WFW	1.5"	No polarizer - 6X zoom shifted about 0.25 inch
WFX	1.5"	Polarizer at 0° - zoom approx. 4X
WFY	1.5"	Polarizer at 45° - zoom approx. 4X
WFZ	1.5"	Polarizer at 90° - zoom approx. 4X
WGA	1.5"	Polarizer at 135° - zoom approx. 4X
WFL	Empty	Empty cavity - no polarizer
WFM	Empty	Empty cavity - polarizer at 0°
WGB	Empty	Empty cavity - polarizer at 0° - zoom approx. 4X
WGC	Empty	Empty cavity - polarizer at 90° - zoom approx. 4X
Table 1. Index of test shots		

4 Data analysis

The raw data were in the form of a phase value for each pixel in the array. These phase values represented the phase of the wavefront which traversed the SiO_2 blank (twice) relative to the planar reference wavefront. Pixels which imaged regions outside of the test sample were turned off, as were pixels for which there was too little light intensity for an accurate phase determination. The data phasefronts contain a linear tilt which was removed by subtracting linear phase gradients in each of two orthogonal directions. The gradient parameters were determined by minimizing the variance of the resultant phasefront.

Table 2 lists the peak-to-valley and r.m.s. variations in the wavefronts. A few conclusions can be drawn from Table 2. First, the r.m.s. phase values of the empty cavity measurements are smaller than the measurements with samples; this indicates that we are seeing a signal above the background noise of the interferometer. Second, the r.m.s. phase value measured for a given sample varies by about a factor of two between measurements. The first four shots listed (WFA, WFB, WFC, WFK) are all of the same sample with circular illumination. Some of this difference may be attributable to thermally induced inhomogeneity, since the pieces were handled between shots. We were able to see thermally induced inhomogeneity on the live monitor during the test when the parts were handled. The rest of the difference may be due to vibration or other noise sources inherent in the test system. A third conclusion to be drawn is that the thick piece of glass distorts less than the thin piece.

Figures 2 and 3 portray wavefronts after two passes through the 3.5 inch and 1.5 inch thick pieces, respectively. In each figure, the upper plot is a three-dimensional contour, and the lower plot is a two dimensional slice across the center of the part. Figure 2 is from shot WFA, Figure 3 is from WFN. The wavefront distortion in these plots is due to the sum of refractive index inhomogeneities and surface figure errors, but birefringence is averaged out, because they were taken with circularly polarized light. Figure 3 shows a circular symmetry to the distortion of the wavefront which traverses the thin piece.

Shot	Piece	Mag	Pol	$\delta\phi_{rms}$ (rad)	$\delta\phi_{p-v}$ (rad)
WFA	3.5"	1X	C	4.2×10^{-2}	2.8×10^{-1}
WFB	3.5"	1X	C	4.0×10^{-2}	2.0×10^{-1}
WFC	3.5"	1X	C	5.6×10^{-2}	3.2×10^{-1}
WFK	3.5"	1X	C	5.9×10^{-2}	3.7×10^{-1}
WFD	3.5"	1X	0	5.5×10^{-2}	3.7×10^{-1}
WFE	3.5"	1X	45	7.0×10^{-2}	4.5×10^{-1}
WFF	3.5"	1X	90	5.6×10^{-2}	4.9×10^{-1}
WFG	3.5"	1X	90	5.5×10^{-2}	4.7×10^{-1}
WFH	3.5"	1X	135	6.4×10^{-2}	4.6×10^{-1}
WFI	3.5"	1X	157.5	7.1×10^{-2}	4.5×10^{-1}
WFJ	3.5"	1X	180	7.8×10^{-2}	4.1×10^{-1}
WGD	3.5"	6X	C	1.1×10^{-2}	1.0×10^{-1}
WFN	1.5"	1X	C	1.0×10^{-1}	5.9×10^{-1}
WFO	1.5"	1X	0	8.8×10^{-2}	6.2×10^{-1}
WFP	1.5"	1X	45	1.1×10^{-1}	7.5×10^{-1}
WFQ	1.5"	1X	90	9.7×10^{-2}	6.9×10^{-1}
WFR	1.5"	1X	135	9.5×10^{-2}	6.9×10^{-1}
WFS	1.5"	1X	157.5	9.1×10^{-2}	6.9×10^{-1}
WFT	1.5"	1X	180	8.9×10^{-2}	6.2×10^{-1}
WFU	1.5"	1X	C	1.0×10^{-1}	7.3×10^{-1}
WFV	1.5"	6X	C	1.6×10^{-2}	1.3×10^{-1}
WFW	1.5"	6X	C	1.1×10^{-2}	2.4×10^{-1}
WFX	1.5"	4X	0	2.4×10^{-2}	2.9×10^{-1}
WFY	1.5"	4X	45	2.7×10^{-2}	2.8×10^{-1}
WFZ	1.5"	4X	90	2.5×10^{-2}	2.9×10^{-1}
WGA	1.5"	4X	135	2.2×10^{-2}	2.9×10^{-1}
WFL	Empty	1X	C	2.2×10^{-2}	1.2×10^{-1}
WFM	Empty	1X	0	2.2×10^{-2}	1.4×10^{-1}
WGB	Empty	4X	0	1.5×10^{-2}	1.9×10^{-1}
WGC	Empty	4X	90	1.6×10^{-2}	2.0×10^{-1}

Table 2. Phase distortion of test shots

We wish to estimate the possible contribution of surface figure error to the phasefront distortion. Figures 4 and 5 show the results of 3-flat tests performed on surface 1 of the 3.5" blank and surface 2 of the 1.5" blank. A 3-flat test is a method for determining the absolute flatness of a line along the diameter of the surface without having to rely on the flatness of a

reference flat.[5] Since the parts were polished together, surface 1 of the 3.5"
blank should be similar to surface 1 of the 1.5", and the surfaces 2 should
likewise look the same. In these figures, the r.m.s. and peak-to-valley values
are expressed in terms of half-wavelengths, so the surfaces conform to a $\frac{\lambda}{50}$
specification in the r.m.s. value of the figure error. Also, both parts are
slightly thinner toward the edges.

The peak-to-valley optical phase distortion due to surface 1 of the 1.5"
part is given by

$$
\begin{aligned}
\delta\phi_{p-v} &= .016\pi \times (1.46 - 1) \\
&= 2.3 \times 10^{-2} \text{ rad.}
\end{aligned}
$$

where the factor of $(1.46 - 1)$ is the difference in refractive index of glass and
air. Surface 2 of the 3.5" part is slightly worse with a $\delta\phi_{p-v} = 3.0 \times 10^{-2}$
radians. The r.m.s. phase distortions of the two measured surfaces are
about the same at $\delta\phi_{rms} = 6 \times 10^{-3}$ radians. Both surfaces contribute to
the wavefront distortion, though their contributions are incoherent. These
surface distortions are about an order of magnitude lower than the peak-
to-valley and r.m.s. distortions measured on transmission, and shown in
Table 2. Therefore, the transmission measurements are measuring volume
inhomogeneity, and not just surface effects.

Autocovariance functions were generated for the wavefronts shown in
Figure 2 and 3. The functions were generated from cuts across each sample,
in the x- and y-directions. The autocovariance function is given by

$$
w(\tau) = \frac{1}{N} \sum_{q=0}^{N} \phi(q)\phi(q + \frac{\tau}{\tau_0}) \tag{1}
$$

where $\phi(q)$ is the phase of the qth pixel along a line, τ is the lag distance, τ_0
is the pixel spacing, and N is the number of pixels along the line. Figure 6
shows autocovariance plots for the 3.5" sample. On each plot is printed the
variance δ and a correlation length α which is the length at which the auto-
covariance drops to 1/e of the variance. Figure 7 contains the corresponding
Fourier transforms. The variances of the different cuts vary by a factor of
two. The correlation lengths range from 1.1 cm to 1.5 cm. Figures 8 and 9
contain autocovariance plots and their transforms for the 1.5" piece.

The birefringence information was analyzed by subtracting phasefronts
measured with light linearly polarized in one direction from phasefronts

---

[5]See Daniel Malacara, ed., *Optical Shop Testing*, 1978.

with light linearly polarized in the orthogonal direction. A benefit of this subtraction procedure is that it eliminates any contribution due to surface figure error from the measured birefringence. This is because the orientation of each part was maintained during each shot as the plane of polarization was varied. Thus, each of the two phasefronts in any subtracted data set contain the same phase distortion due to surface errors, and that surface effect is cancelled.

Figures 10 and 11 show phasefronts from the 3.5" piece in vertical and horizontal light, respectively, and Figure 12 shows the relative phasefront, i.e., Figure 11 subtracted from Figure 10. The notched area in the foreground of Figure 11 represents an area for which the interferometer did not record data, possibly because the light intensity on the interferometer CID array was near its detection threshold for the shots taken through a linear polarizer. The variance of the difference phasefront shown in Figure 12 is 5.7×10^{-3} rad^2. The peak-to-valley is .52 radians. Figure 13 shows a difference phasefront for the same glass sample made from shots polarized at 45° and 135° from vertical. It's variance is 7.8×10^{-3} rad^2, and its peak-to-valley is .48 radians. The mean values of the phasefronts in Figures 12 and 13 are 6.2×10^{-3} and 3.3×10^{-3} radians, respectively, but caution must be used in the interpretation of these mean values. While they might represent a uniform birefringence over the entire sample, they might also be artifacts of the algorithm used to remove the tilt from the wavefronts. The Zygo interferometer does not give one an absolute reference phase, so the determination of a non-varying birefringence from the subtraction of two phasefronts is difficult.

The 3.5" sample shows quite a bit of structure in the birefringence plots near the hole. This could be the result of stress induced during the drilling process, although the last annealing of the part was done after the hole was drilled.

Figures 14 and 15 are phasefronts from the 1.5" piece in vertical and horizontal light. Figure 16 is the difference in the phasefronts. the peak-to-valley of the phasefront in Figure 16 is .27 radians, less than either of the phasefronts in Figures 14 and 15. This is a result of the subtraction of the high index region around the edge of the piece. The variance of the difference phasefront is 1.2×10^{-3} rad^2, and the mean value is 2.7×10^{-3} radians. Figure 17 is a difference phasefront of the same sample from shots taken in light polarized at 45° and 135° from vertical. It's variance is 6.8×10^{-4} rad^2, mean is -3.6×10^{-3} radians, and peak-to-valley is .23 radians. The periodic structure in Figures 16 and 17 is indicative of a periodic, non-isotropic stress

in the material.

Although Figures 12, 13, 16, and 17 show pixel-by-pixel phasefront differences, we averaged groups of four pixels together when computing the autocovariance functions of the difference phasefronts. This was done to minimize the effect of any registration error in the subtraction process. The autocovariance functions of the 3.5 inch piece are shown in Figures 18 and 19. Figure 18 was computed from the difference of the phasefronts measured in vertically and horizontally polarized light. Figure 19 was computed from the difference of the phasefronts measured in light polarized at 45o and 135° from vertical. In both sets of figures, "columns" are vertical (0°) cuts through the data, and "rows" are horizontal cuts. Figures 20 and 21 are the corresponding power spectra. There is a very noticeable periodicity in the vertical direction. The magnitude is polarization-dependent, which is why it shows up in these difference phasefronts, but not in Figures 6 and 7. This periodicity is quite visible in Figures 16 and 17, and barely visible in Figures 14 and 15.

Figures 22 through 25 show the autocovariance functions and power spectra computed from the difference phasefronts of the 1.5" substrate. The unidirectional periodicity which is visible in Figures 16 and 17 appears as the periodicity in the columnar autocovariance functions and the peak in the corresponding power spectra. The spatial frequency of the periodicity is slightly greater than 0.5 cm^{-1}, and the peak amplitude of its Fourier component varies across the part. This variability is evident in Figures 16 and 17.

Figures 26 and 27 are histograms of the difference between the $x-$ and $y-$components of refractive index for the two blanks. As discussed above, the offset from zero of the peaks in these two blanks may be an artifact of the lack of a reference phase in the data, but the width of the histogram distribution is an accurate reflection of the variability of the birefringence across the part.

5 Effect of inhomogeneity and birefringence in interferometers

The inhomogeneity and birefringence of fused silica blanks will result in distortion of the wavefront propagating through an interferometer, which leads in turn to loss of contrast and power. This section presents the results of numerical calculations of the contrast which can be expected in LIGO if

inhomogeneity and birefringence are the limiting factors.

5.1 Direct calculation

Data from the 3.5 inch blank could not be used directly in a contrast cal-
culation, because the blank has a hole through its center. The 1.5 inch
blank has no such restriction, and the calculation assumes two blanks, one
represented by the horizontal polarization and vertical polarization phase-
fronts (WFO and WFQ), and the other by the 45° and 135° phasefronts
(WFP and WFR). A circularly polarized Gaussian beam of 2.15 cm waist
radius was assumed to make two passes through one of these blanks, and an
identical beam was assumed to traverse the other. The contrast expected
from the two blanks was calculated. Table 3 displays the result of these
calculations. The second column shows the contrast one would expect from
the 1.5 inch blank data, and the third column shows the contrast one would
expect if the thickness and wavelength were scaled to 10 cm and half micron,
respectively. This scaling assumes that column inhomogeneity and birefrin-
gence scale linearly with thickness, a conservative assumption. The first row
shows the contrast expected from a blank representing the 0°-90° data and
a blank representing the 45°-135° data. The isotropic index inhomogeneity
cancels out in this calculation, so the contrasts represent degradation due
to birefringence only. The second row shows contrasts from the same two
blanks, but with one rotated 90° about the optic axis. Both inhomogeneity
and birefringence contribute to the loss of contrast in this example. The
third and fourth rows show contrasts from the two blanks with one shifted
by one and three cm relative to the other.

	Contrast	Contrast with scaling
0°-90° vs 45°-135°	0.999	0.988
0°-90° vs 45°-135°, 45°-135° rotated 90°	0.996	0.960
0°-90° vs 45°-135°, 45°-135° shifted 1 cm	0.998	0.980
0°-90° vs 45°-135°, 45°-135° shifted 3 cm	0.985	0.927
Table 3. LIGO contrasts derived from 1.5 inch sample.		

It is worth bearing in mind that the 1.5 inch blank has a large refrac-
tive index inhomogeneity, and the contrast limits due to inhomogeneity and
birefringence we may expect in LIGO are not as severe as Table 3 implies. If
the same calculation were possible with the 3.5 inch blank, better contrast
would result.

5.2 Monte Carlo simulation

A monte carlo simulation of LIGO-scale mirrors has been carried out to determine what the loss of contrast is likely to be in LIGO. Data from the 3.5 inch test blank was used to determine the parameters for a model, and computer-generated mirrors were used to estimate the possible range of contrasts.

The mirrors were modeled to have a Gaussian distribution of refractive index inhomogeneity.[6] The model is a two-dimensional grating in which the wave vector components are given random phases. The relative strength of the wave vector components is given by the *surface factor*, which is the Fourier transform of the autocovariance of the inhomogeneity. The surface factor is

$$g(k) = \pi\delta\alpha^2 e^{-\frac{k^2\alpha^2}{4}} \tag{2}$$

where δ is the phase variance, α is the correlation length, and k is the wave vector of the Fourier component of the inhomogeneity. An isotropic inhomogeneity distribution was generated first, then a birefringence distribution was added, using the same model with different parameters. Vertical and horizontal were maintained as the principal axes of the birefringence throughout.

The correlation lengths used in the model were chosen to mimic those seen in the data from the 3.5 inch blank. Various cuts through the measured phasefront show correlation lengths of refractive index inhomogeneity in the 1 to 2 cm range, and 1.75 cm was used in the model. 3.5 cm was used as the birefringence correlation length.

The choice of amplitude of inhomogeneity and birefringence is more difficult. Only two samples of glass were measured, and the thinner has a greater amplitude of inhomogeneity, indicating some problem in its manufacture. Thus, we do not know how inhomogeneity scales with thickness. If the inhomogeneity and birefringence are truly random in three dimensions, and if the correlation length along the optical axis is less than the blank thickness, then the inhomogeneity ought to scale with the square root of the thickness. This was chosen for one of two trials. For the other, the more conservative assumption of linear scaling of inhomogeneity and birefringence with thickness was used.

In the 3.5 inch (8.9 cm) blank, the rms inhomogeneity was measured to be

---

[6]See Elson and Bennett, *Relation between the angular dependence of scattering and the statistical properties of optical surfaces*, J. Opt. Soc. Am., v.69, n.1, January 1979

.06 radians, and the rms birefringence was .08 radians. These numbers were multiplied by the ratio of the LIGO wavelength to the test wavelength. The LIGO mirror thickness was taken to be 14 cm, so the rms amplitudes were multiplied by the ratio of thicknesses in one case, and by the square root of that ratio in the other. For the linear scaling model, the rms inhomogeneity was .12 radians, and the birefringence rms was .17 radians. For scaling with the square root of thickness, the rms inhomogeneity was .10 radians, and the birefringence rms was .12 radians. These numbers are summarized in Table 4.

	3.5 inch Data (rad)	$\sqrt{\delta} \propto l$ Model (rad)	$\sqrt{\delta} \propto \sqrt{l}$ Model (rad)
Rms inhomogeneity	.06	.12	.10
Rms birefringence	.08	.17	.12
Table 4. Comparison of data and Monte Carlo models.			

Figure 28 shows the profile of a wavefront generated in this simulation. Figure 29 shows autocovariance functions and power spectra for the horizontal and vertical diameters of the same blank. The projection of the refractive index ellipsoid of each pixel into the horizontal direction was used in Figure 29. The gross features of the autocovariance functions and their Fourier transforms match those of the test data.

To calculate the contrast in a LIGO made with such mirrors, ten distorted wavefronts were generated corresponding to two passes of a 2.15 cm radius, circularly polarized Gaussian beam through ten mirrors generated according to the same model. The only difference between the ten simulated mirrors was in the random phases assigned to the Fourier components of the inhomogeneity. The maximum and minimum intensities from all possible pairs of the ten wavefronts was then calculated by summing and squaring the phasefronts. Phase difference information between the horizontal and vertical components of the electric field was maintained. The contrast was then calculated to be the difference between maximum and minimum intensities divided by their sum. For each set of ten mirrors there are forty-five possible combinations. Figure 30 shows histograms of the resultant contrasts for the two trials. For inhomogeneity scaling linearly with thickness, the range of contrasts is .989-.999 with an average value of .996. For scaling with the square root of thickness, the range is .991-.999 with an average value of .998.

Beyond the value of the contrast derived, this result is significant because

11

it indicates that different pairs of mirrors can give different results, even though the mirrors are statistically similar. The orientation of the mirrors in a given pair around the interferometer optic axis may also affect the contrast. A simulation using inhomogeneity data only (no birefringence) shows this to be the case.

A contrast estimate was made for the forty meter prototype with monolithic mirrors. In this case, the rms inhomogeneity was taken to be .11 radians, and the rms birefringence was taken to be .12 radians. The resultant range of contrasts was found to be .992-.999 with an average value of .998. However, the extrapolation of the Zygo data to the small spot sizes of prototype interferometers is not as sound as it is for LIGO spot sizes, because the pixel spacing is only three times smaller than the spot radius, and fine structure which might affect prototypes more than LIGO does not appear.
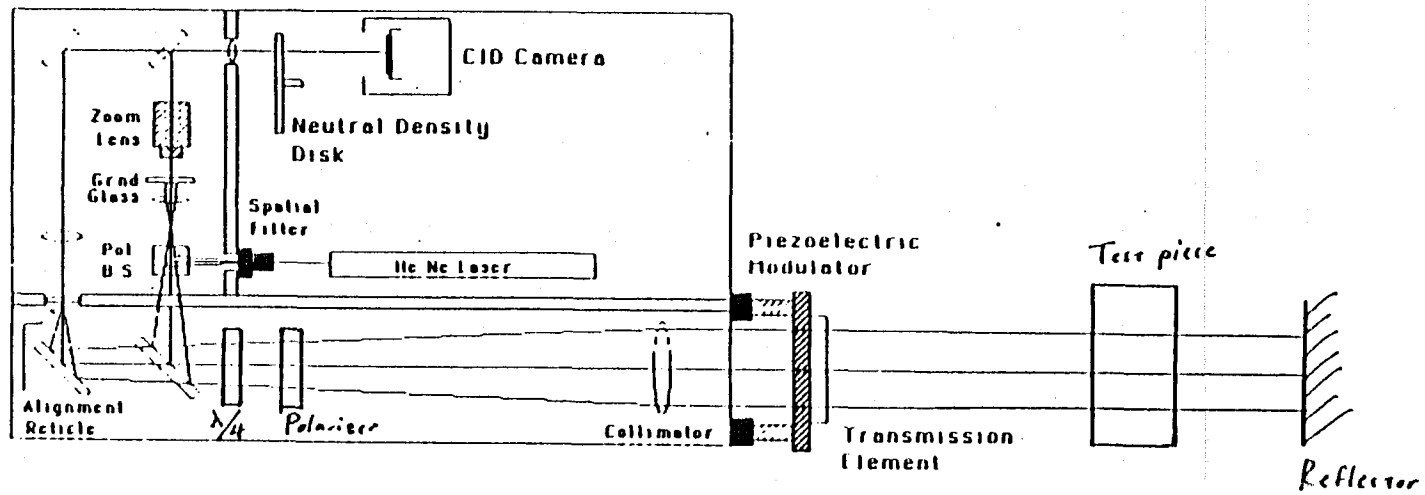
Figure 1.   Schematic of the Zygo Interferometer.
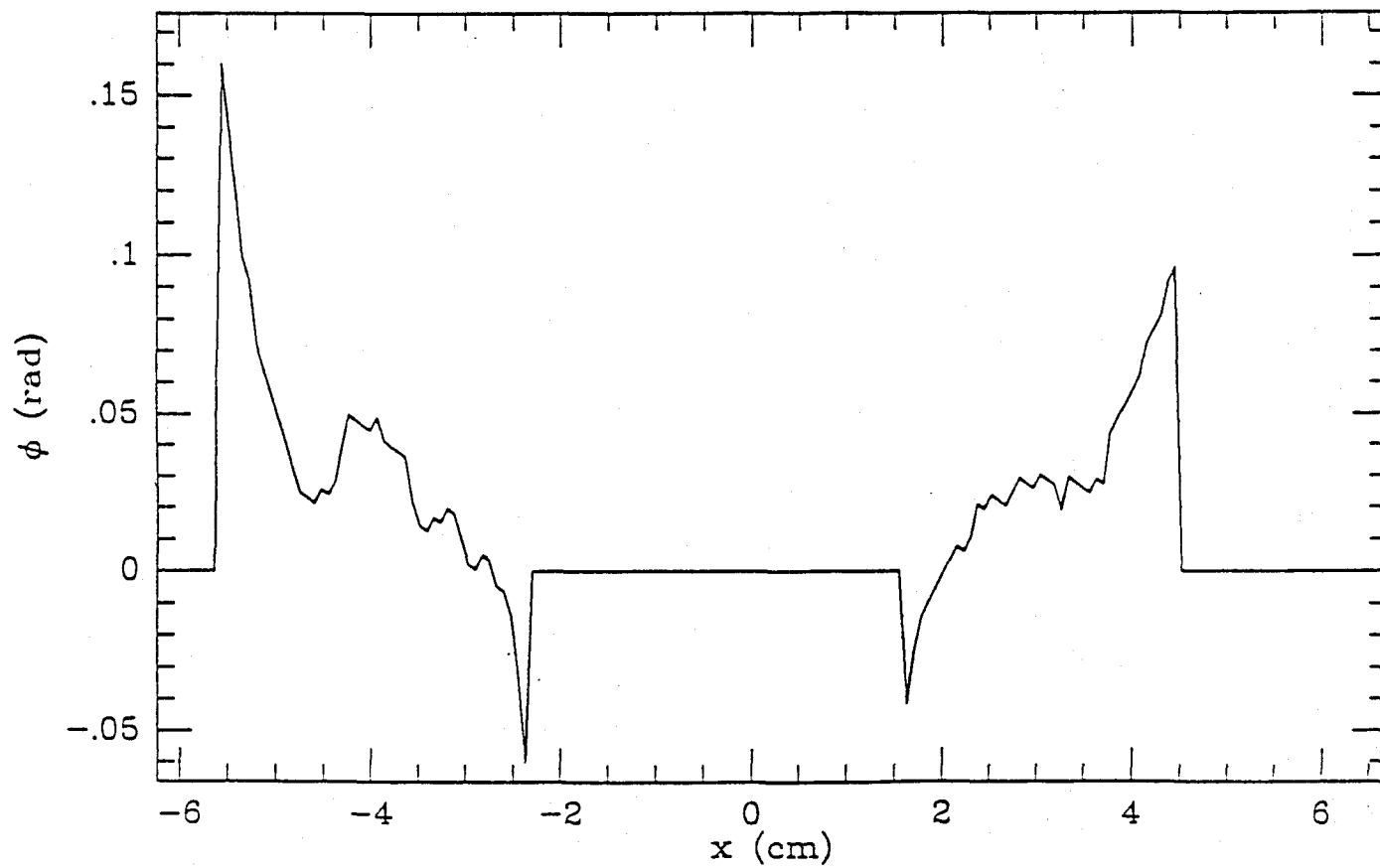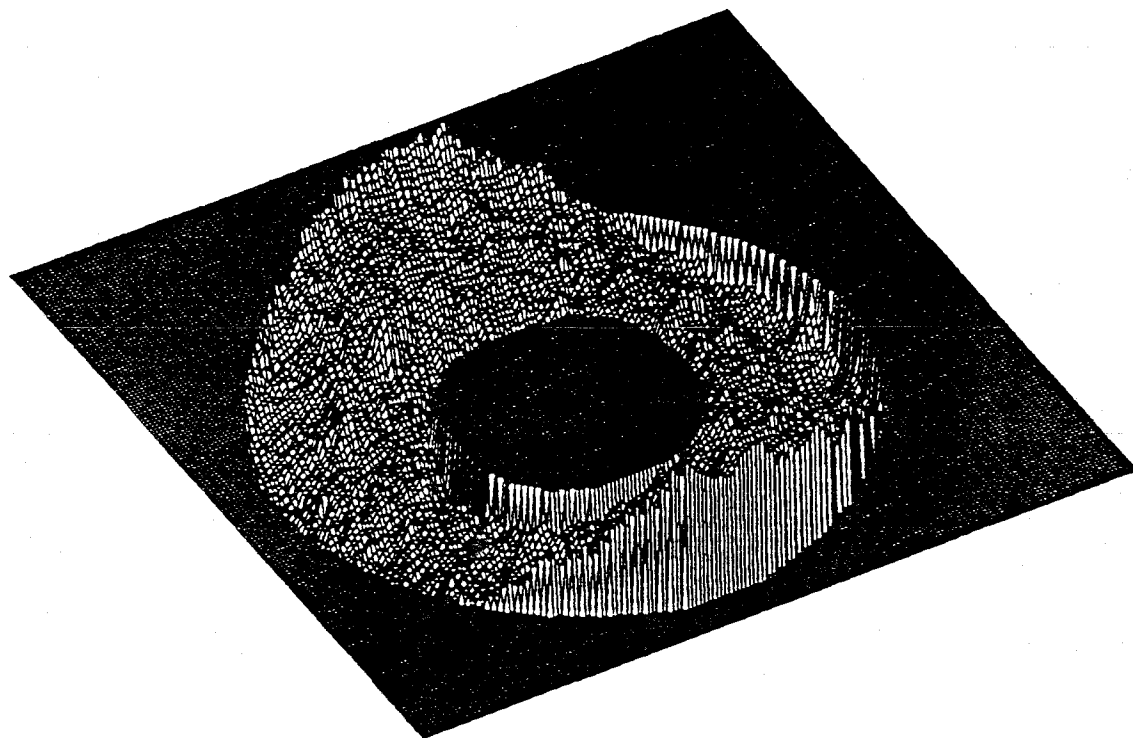
Figure 2.   The 3.5 inch test piece in circularly polarized light.
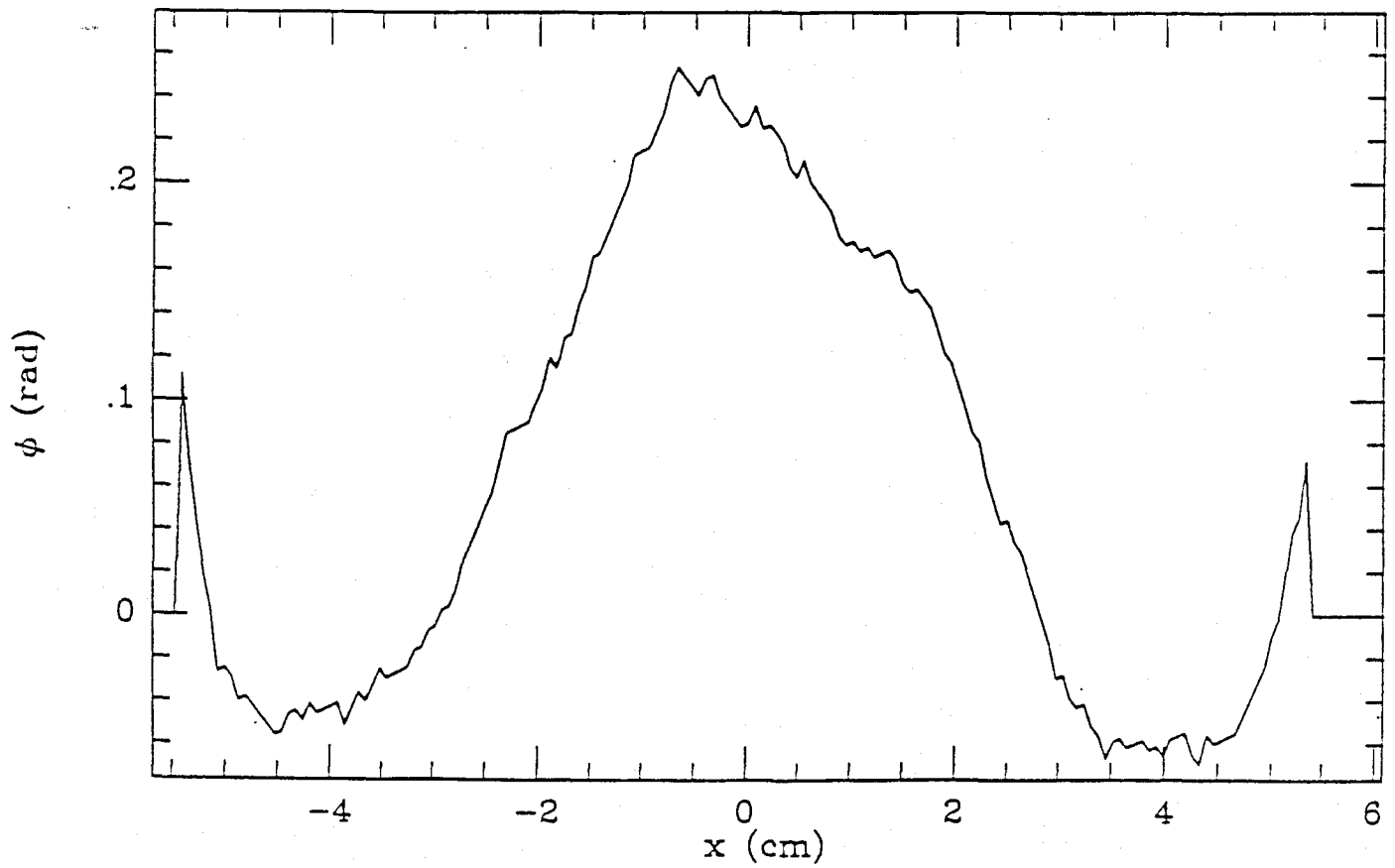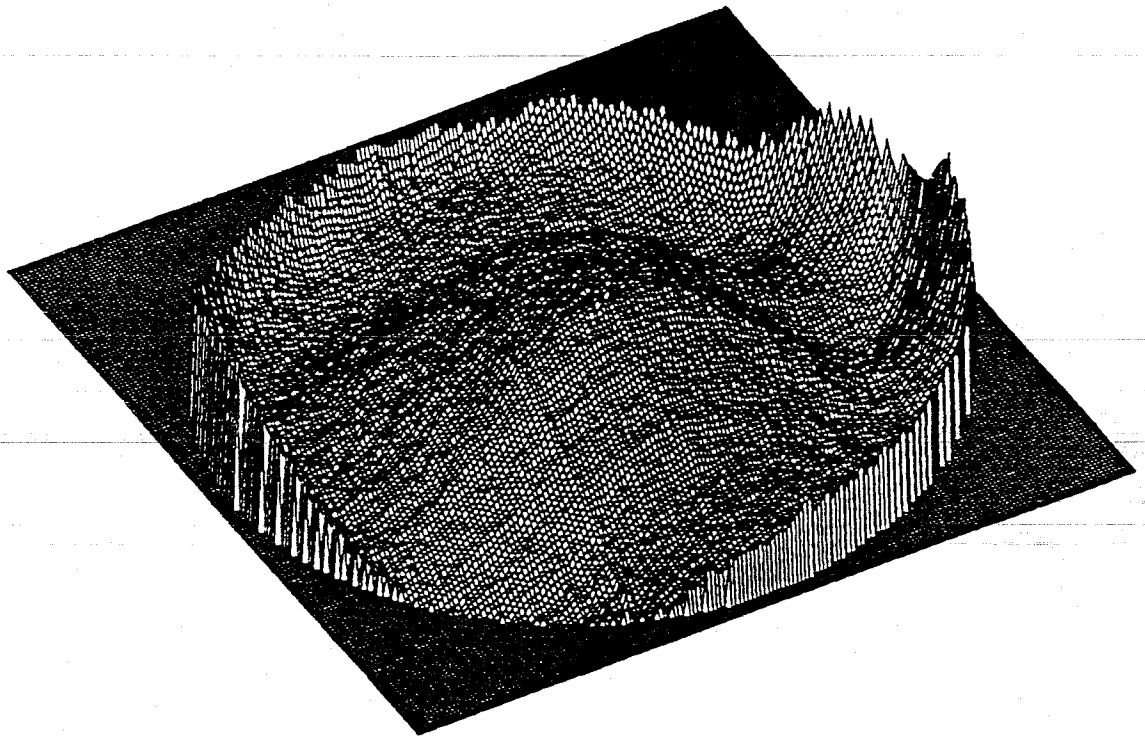
Figure 3. The 1.5 inch test piece in circularly polarized light.

Figure 4.

*** THREE FLAT TEST ***

14-NOV-1998/12:38:53   No of meas : 18   RMS : 0.004
III : NOT FLAT   Trim : 2
S/N : ERE   Waveout : 0.6328
Max= 0.005
PV= 0.021
Min= -0.016

Vertical Diameter

Max= 0.004
PV= 0.017
Min= -0.013

Horizontal Diameter

Cust. _____MIT_____ P/N _____—_____ Rev. —
Item _____ES FLAT_____ S/N _____—2_____
W.O. _____M128310_____ Clear Ap. _____92%_____
S/F _____1F = λ/2_____ W/L _____6328A_____ Coated _____
Test _____ABSOLUTE_____ A.O.I. _____0°_____ Uncoated _____✓_____
Emp. _____640_____ Date _____11/14/98_____   ZYGO

Figure 5.

$\delta=5.87\text{E}-04 \ \ \text{rad}^2$
$\alpha=1.11 \ \ \text{cm}$
Row 48

$G(\tau) \ (\text{rad}^2)$

$\tau_x \ (\text{cm})$

$\delta=7.02\text{E}-04 \ \ \text{rad}^2$
$\alpha=1.41 \ \ \text{cm}$
Row 115

$G(\tau) \ (\text{rad}^2)$

$\tau_x \ (\text{cm})$

$\delta=9.28\text{E}-04 \ \ \text{rad}^2$
$\alpha=1.48 \ \ \text{cm}$
Column 48

$G(\tau) \ (\text{rad}^2)$

$\tau_y \ (\text{cm})$

$\delta=4.41\text{E}-04 \ \ \text{rad}^2$
$\alpha=1.34 \ \ \text{cm}$
Column 115

$G(\tau) \ (\text{rad}^2)$

$\tau_y \ (\text{cm})$
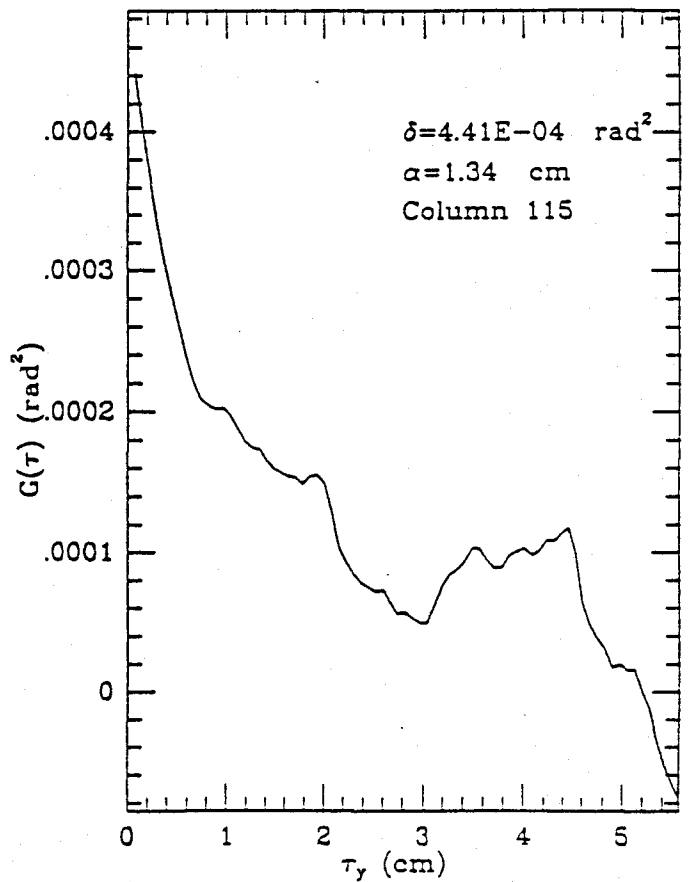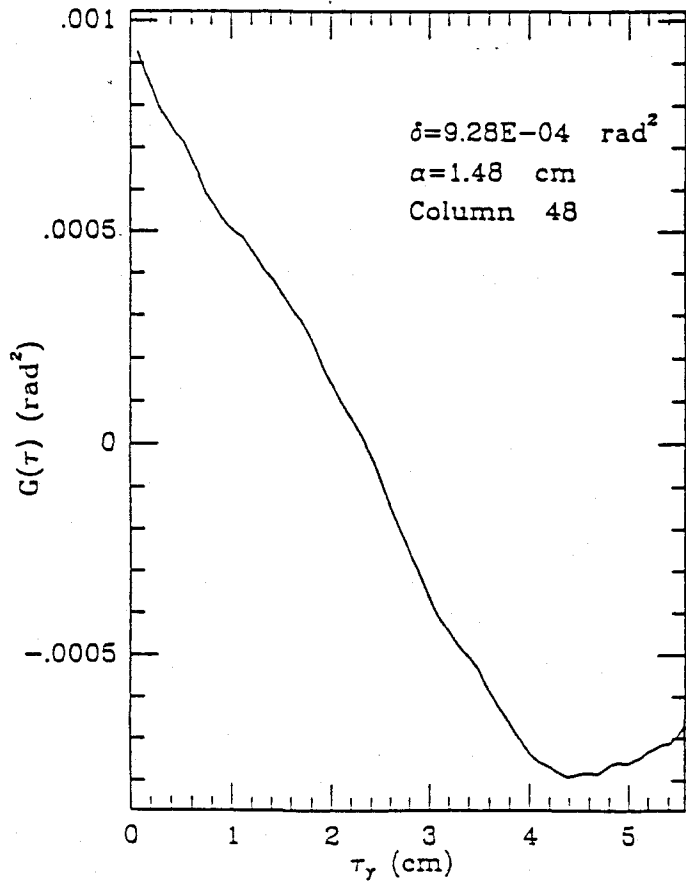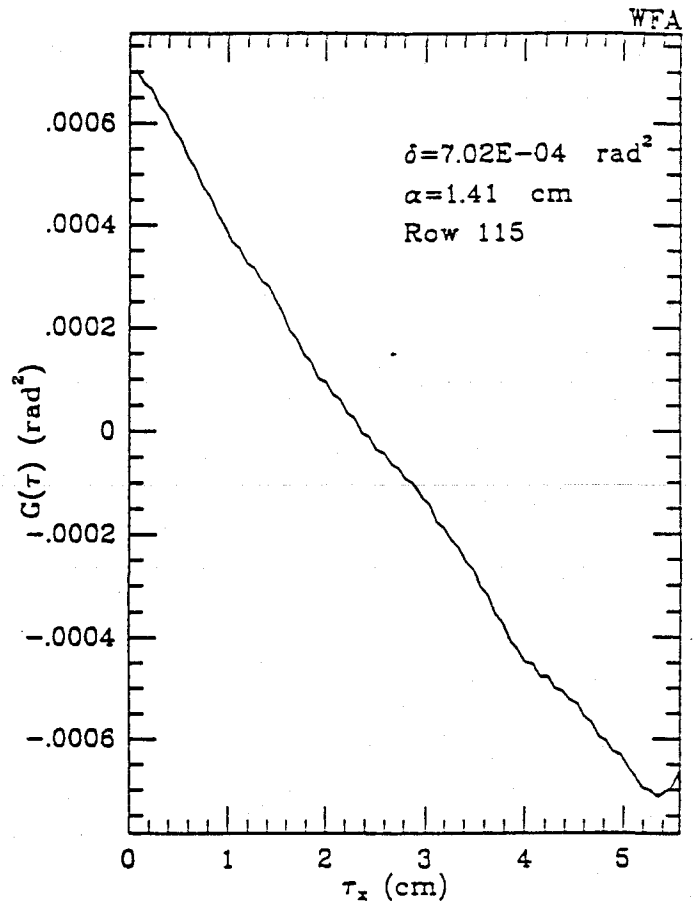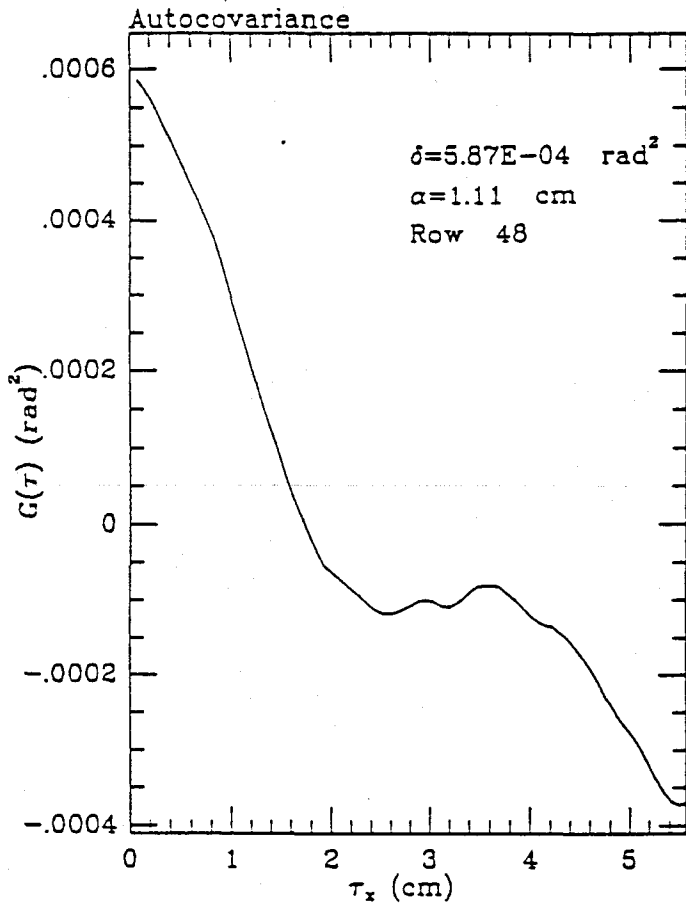
Figure 6. Autocovariance plots for the 3.5 inch test piece in circularly polarized light.
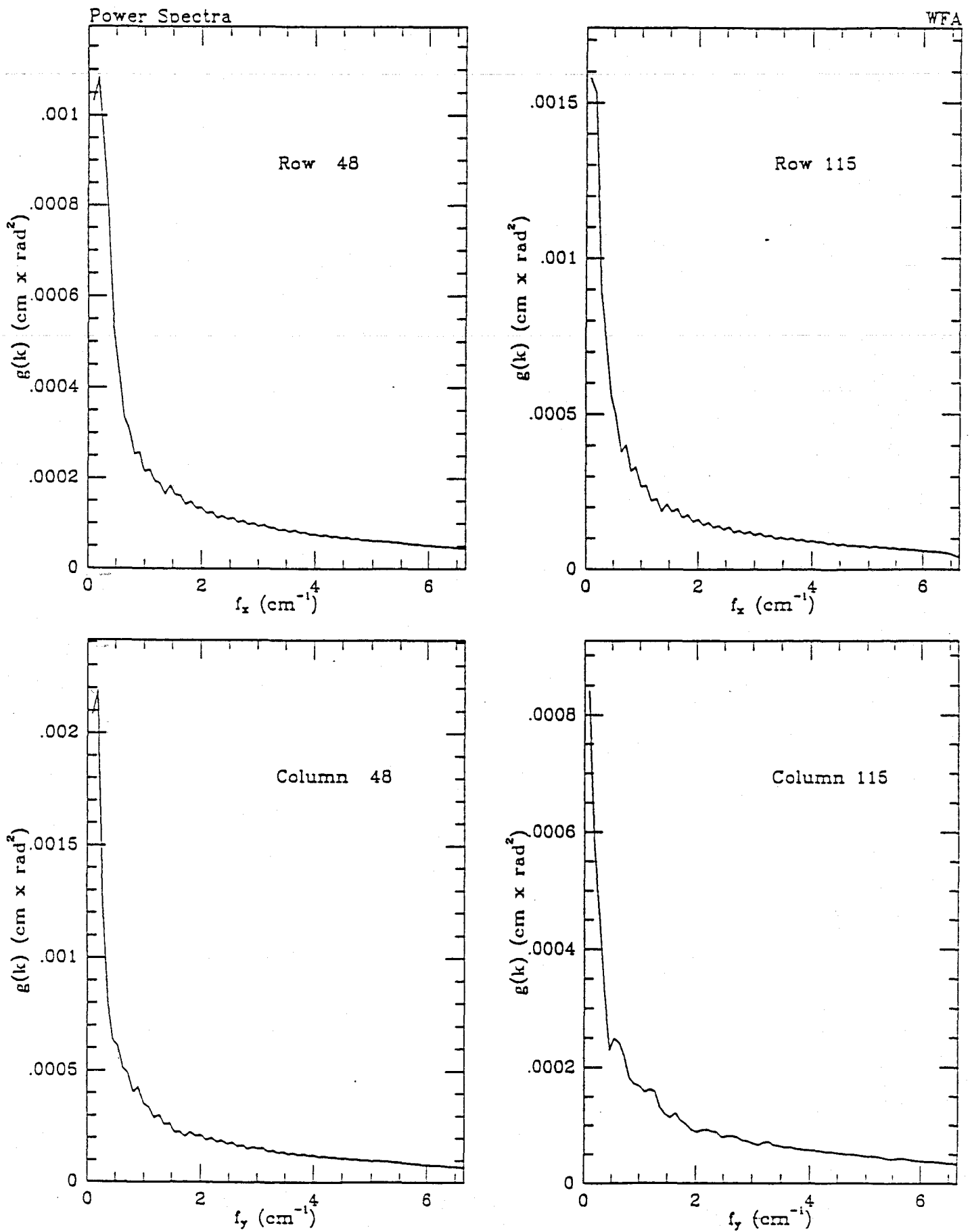
Figure 7.   Fourier transforms of the autocovariance functions of the 3.5 inch
test piece in circularly polarized light.

$\delta=1.01E-02$ rad^2
$\alpha=1.49$ cm
Row 48

$\delta=7.16E-03$ rad^2
$\alpha=1.08$ cm
Row 115

$\delta=1.01E-02$ rad^2
$\alpha=1.69$ cm
Column 48

$\delta=7.17E-03$ rad^2
$\alpha=1.76$ cm
Column 115
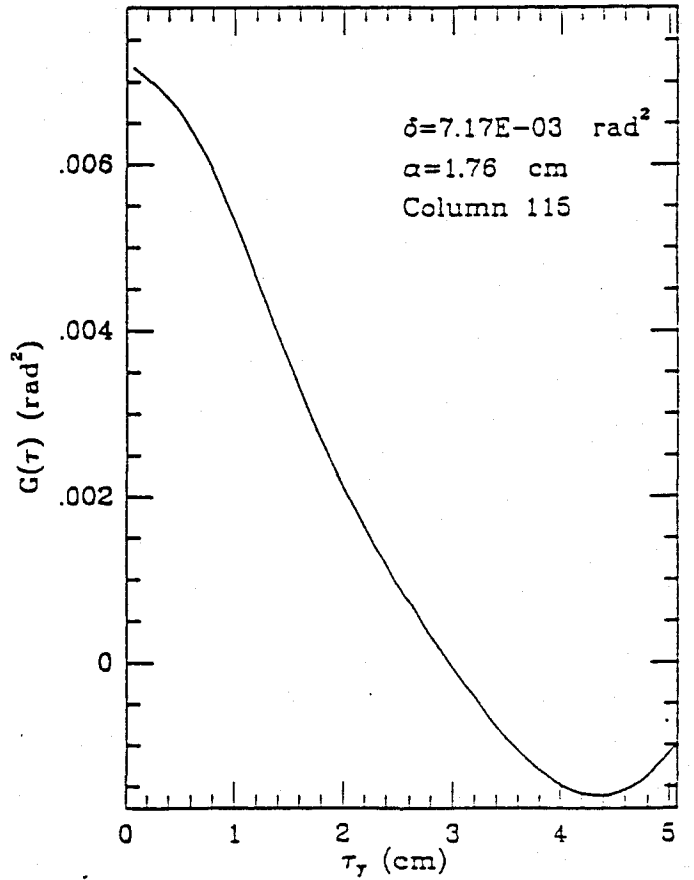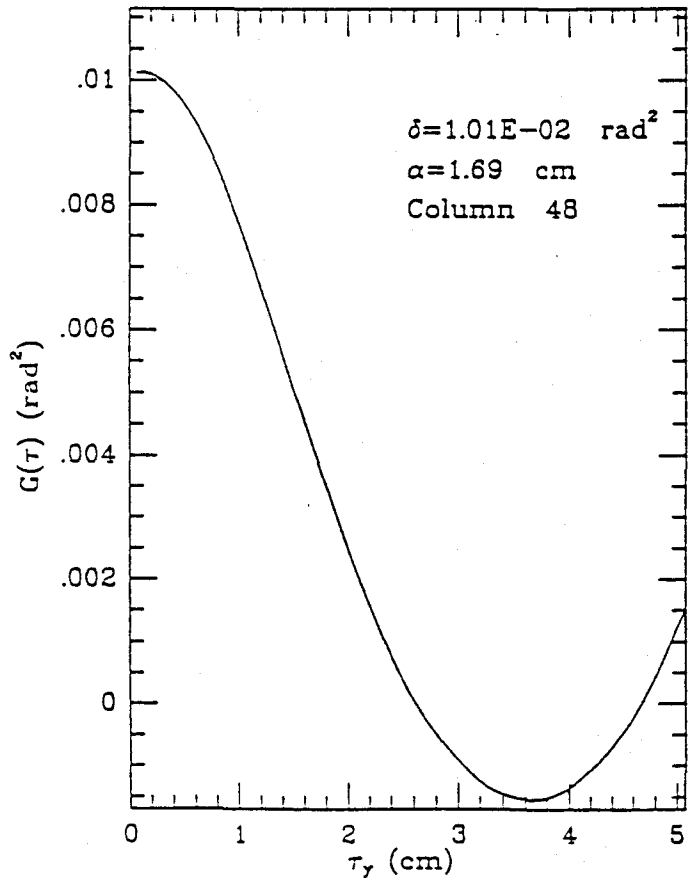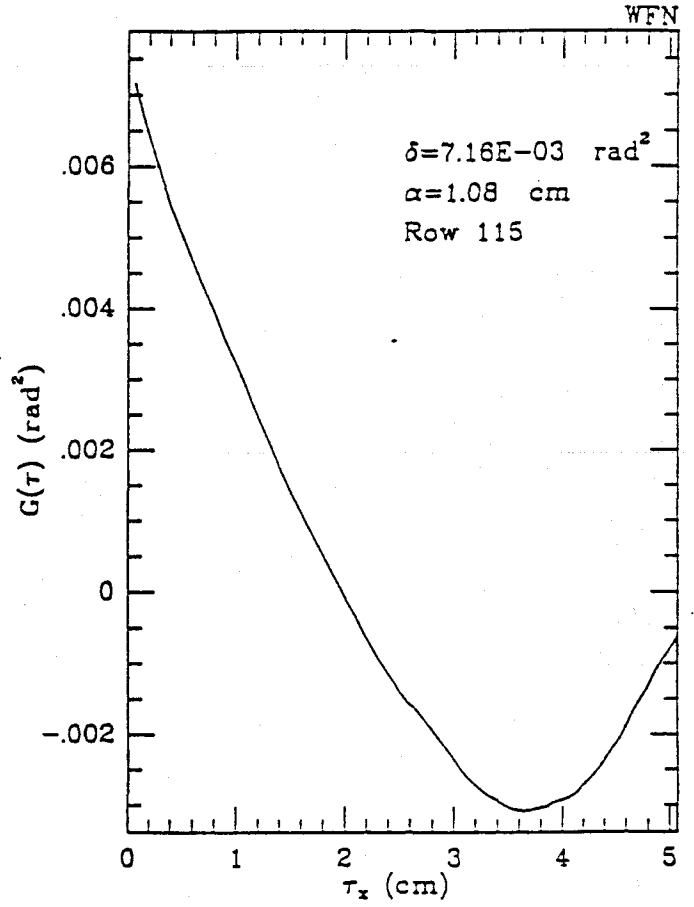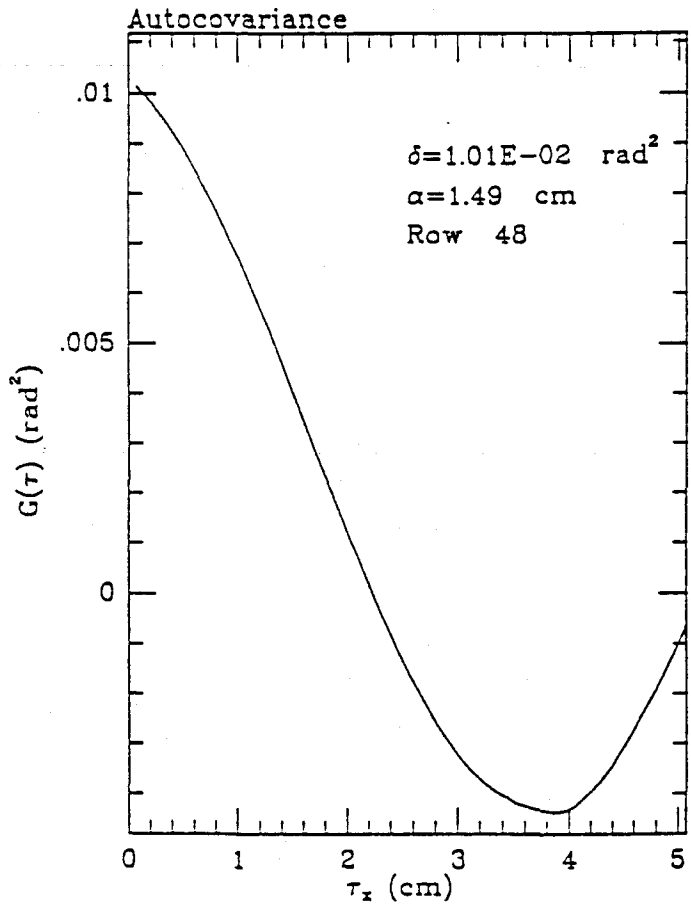
Figure 8.   Autocovariance functions of the 1.5 inch test piece in circularly
polarized light.
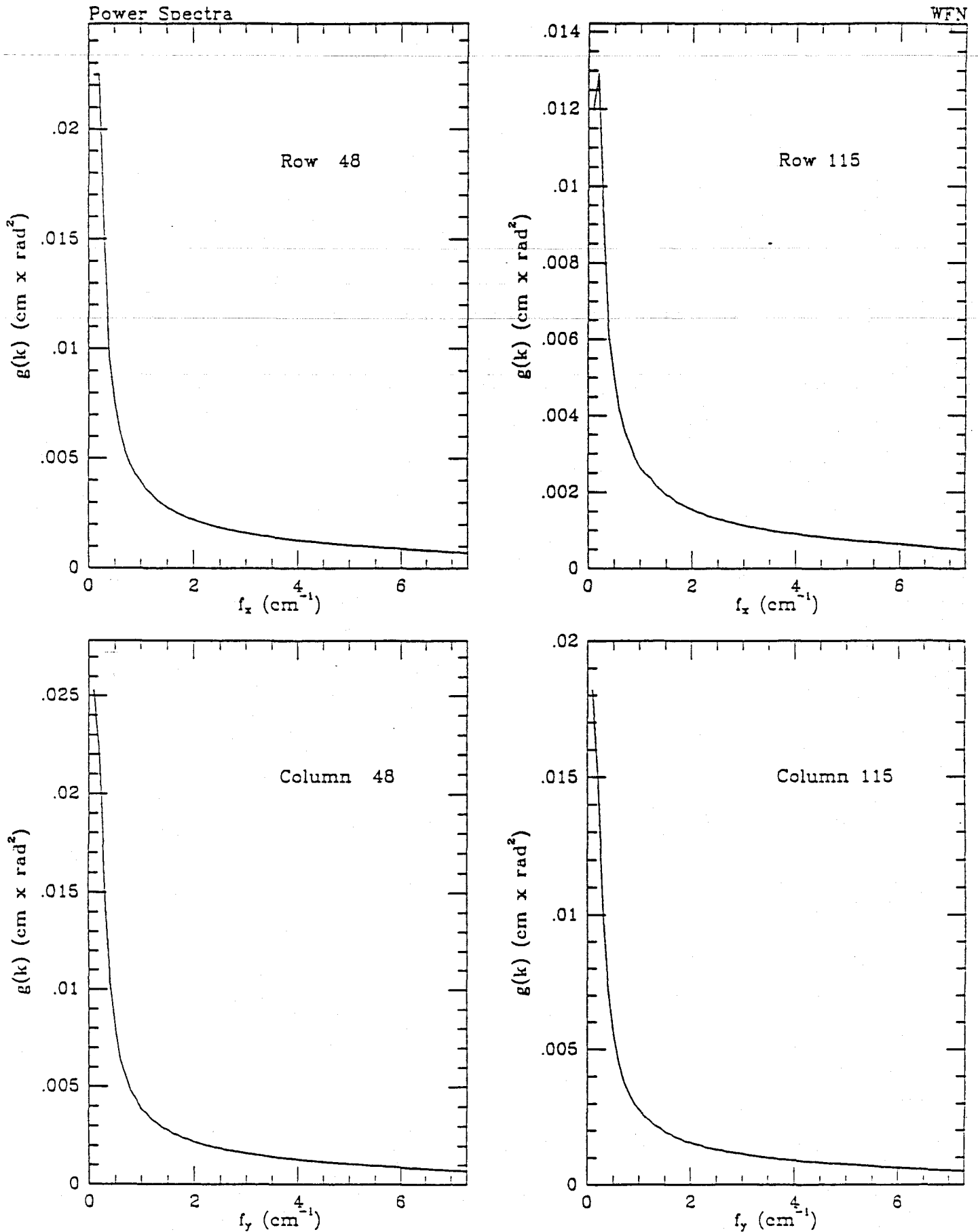
Figure 9.   Fourier transforms of the autocovariance functions of the 1.5 inch
            test piece in circularly polarized light.
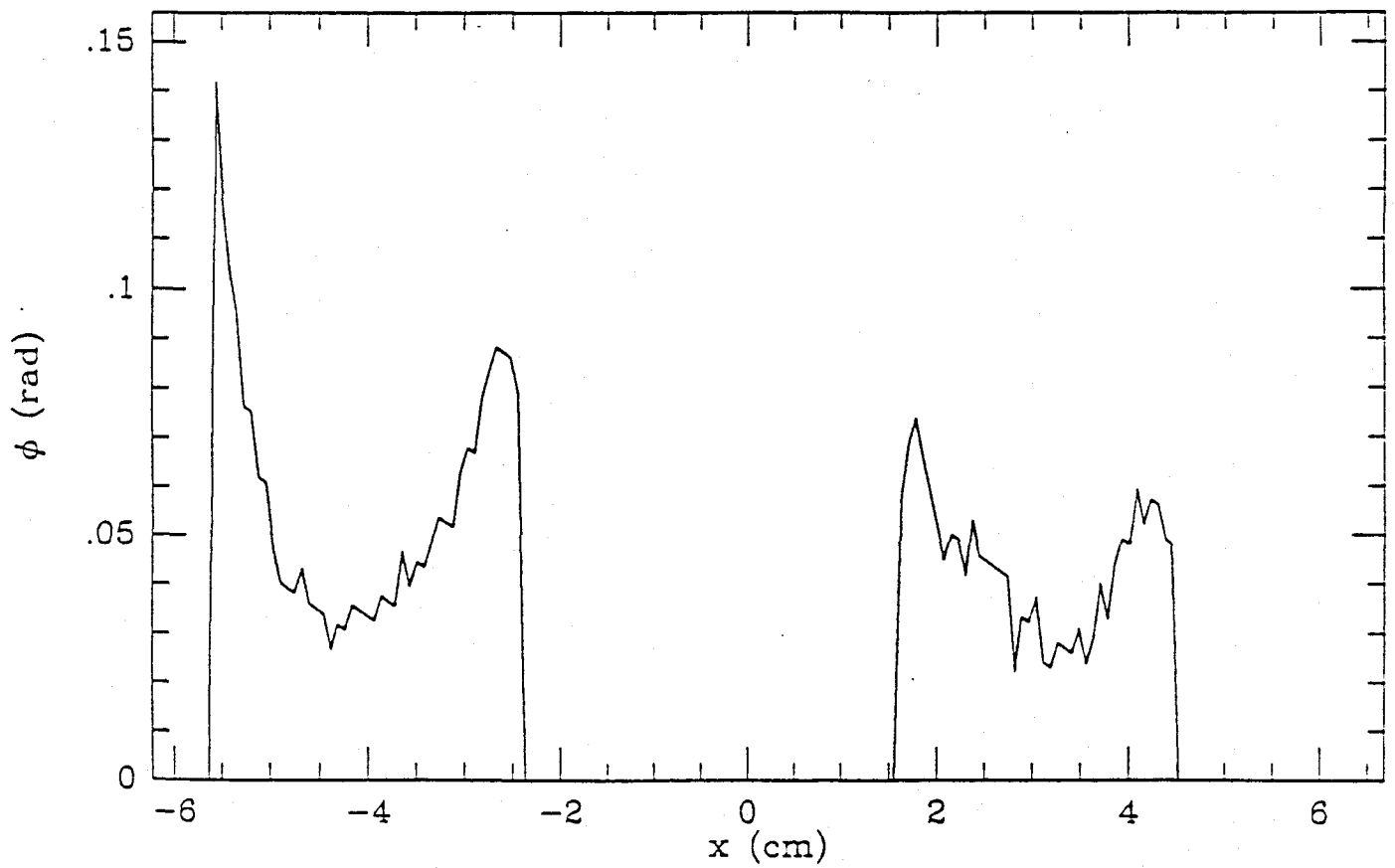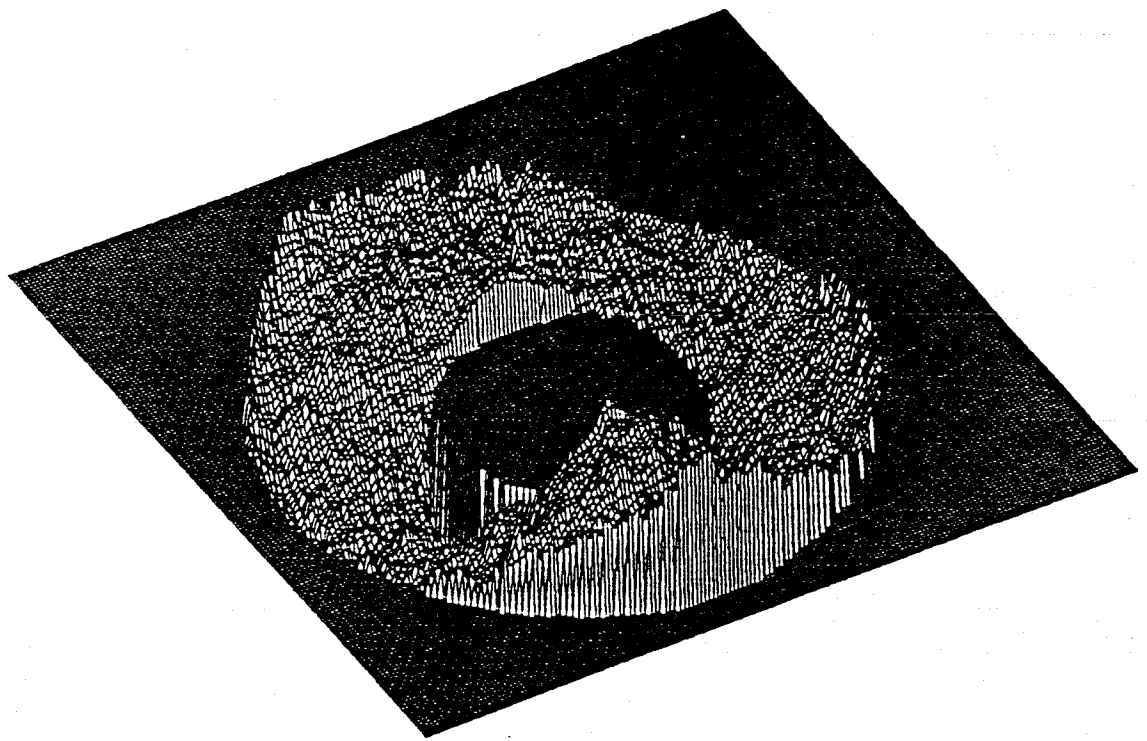
Figure 10.   The 3.5 inch test piece in vertically polarized light.
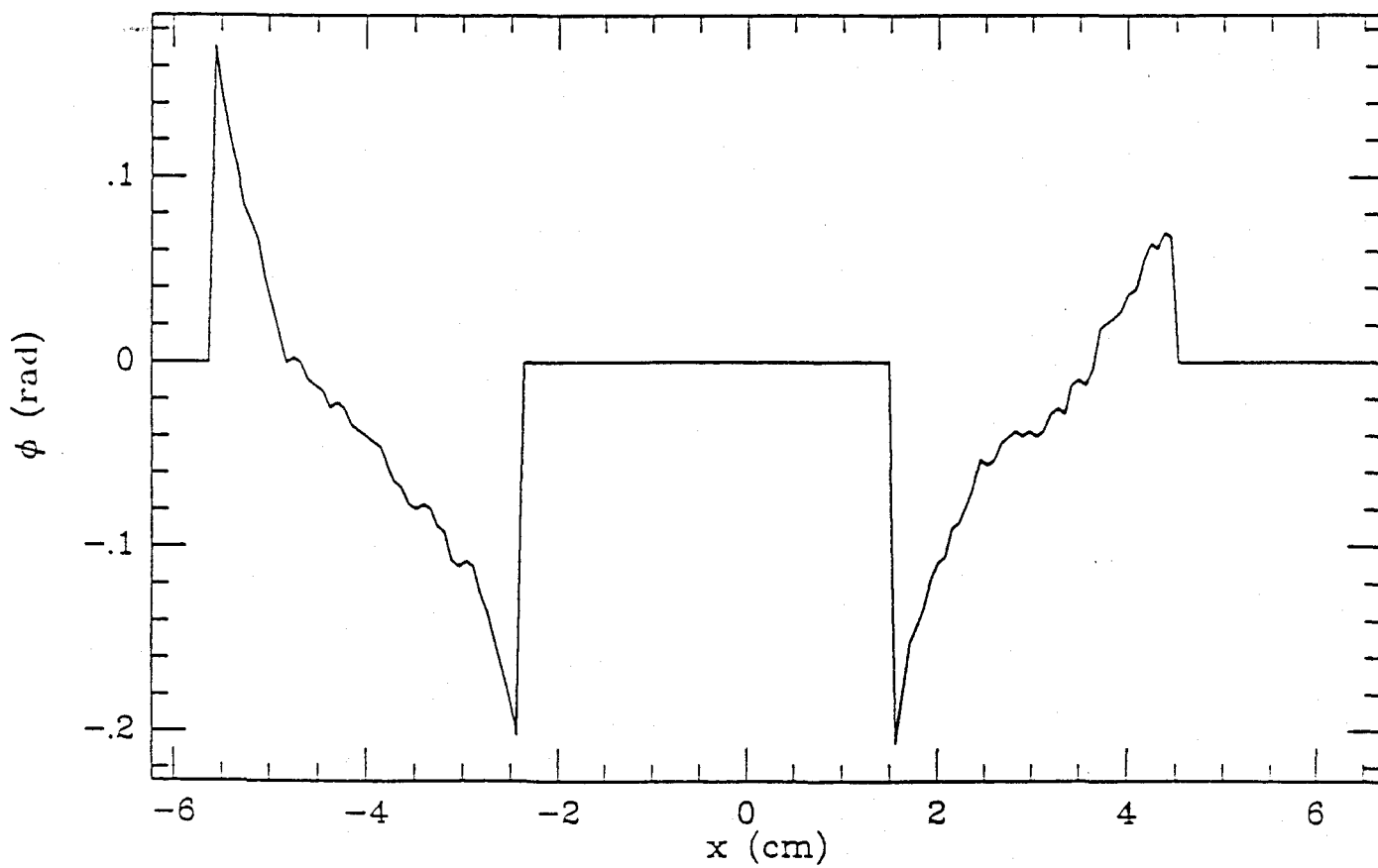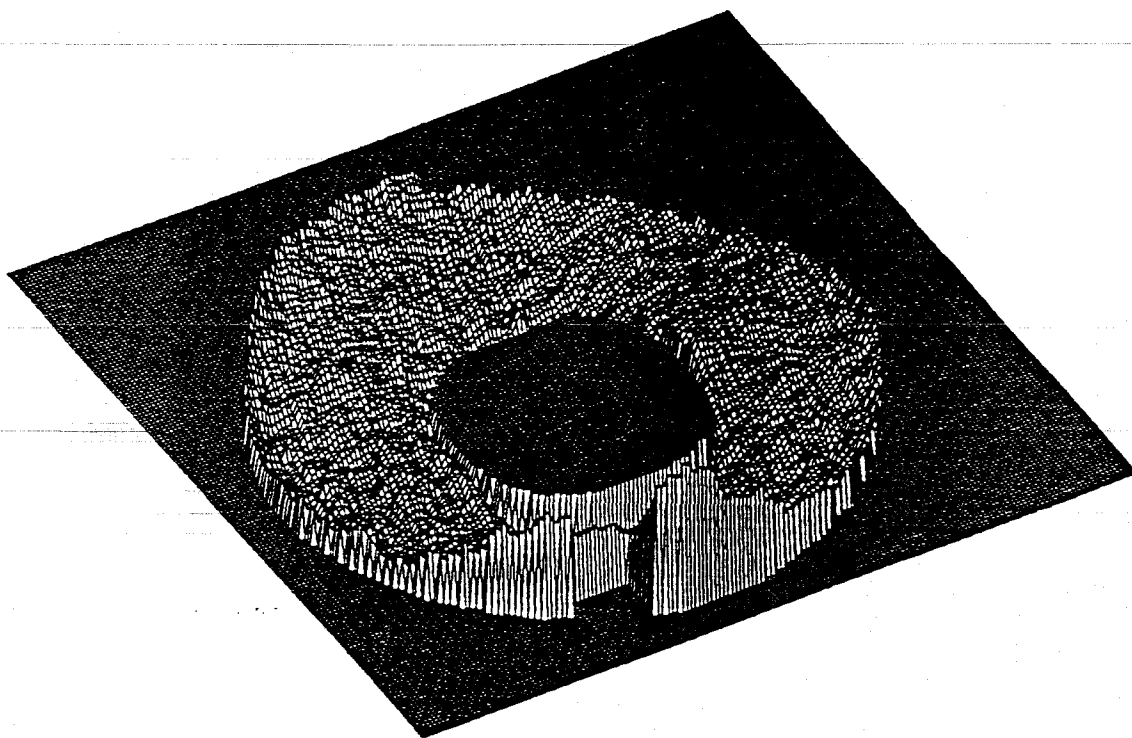
Figure 11. The 3.5 inch test piece in horizontally polarized light.
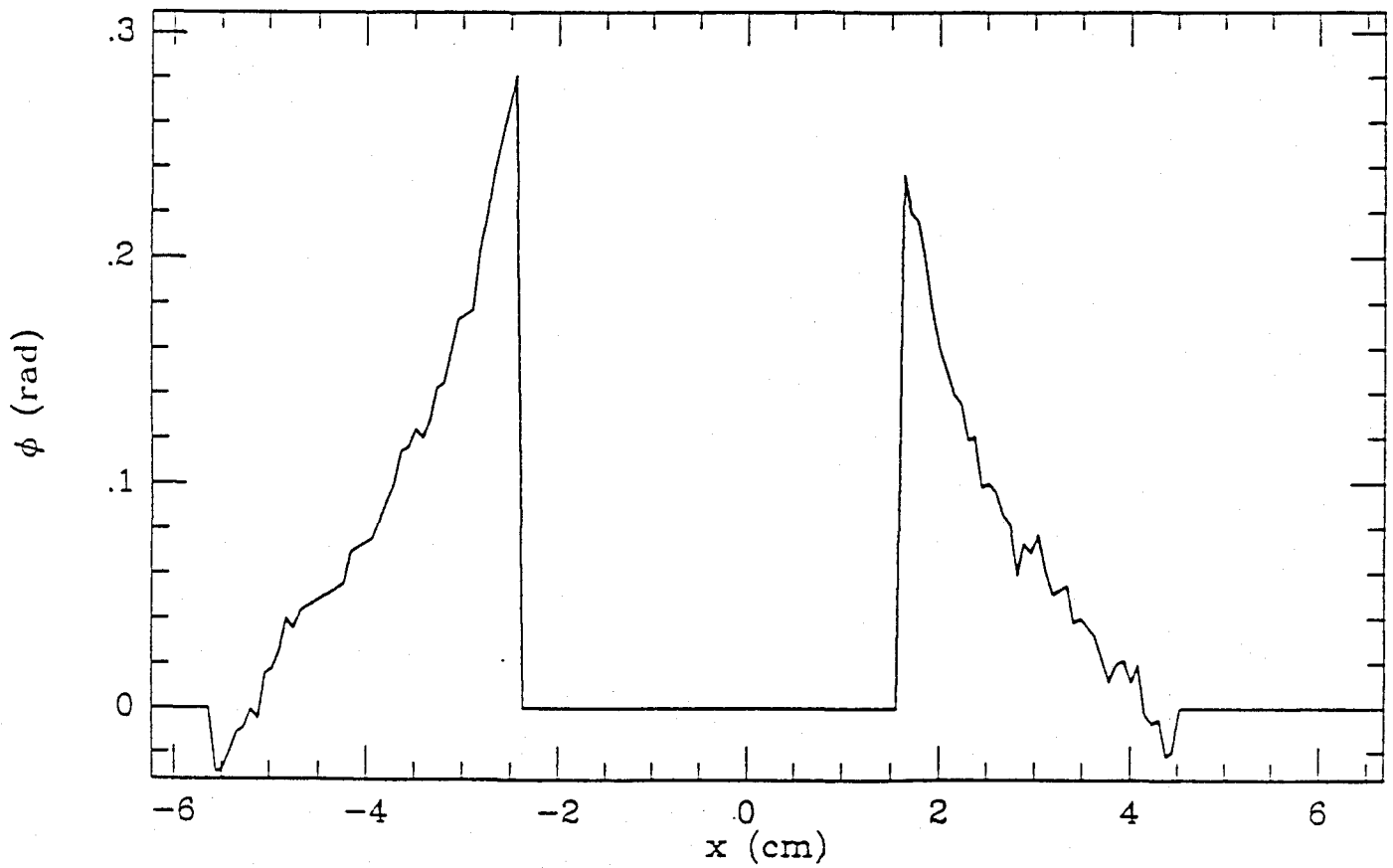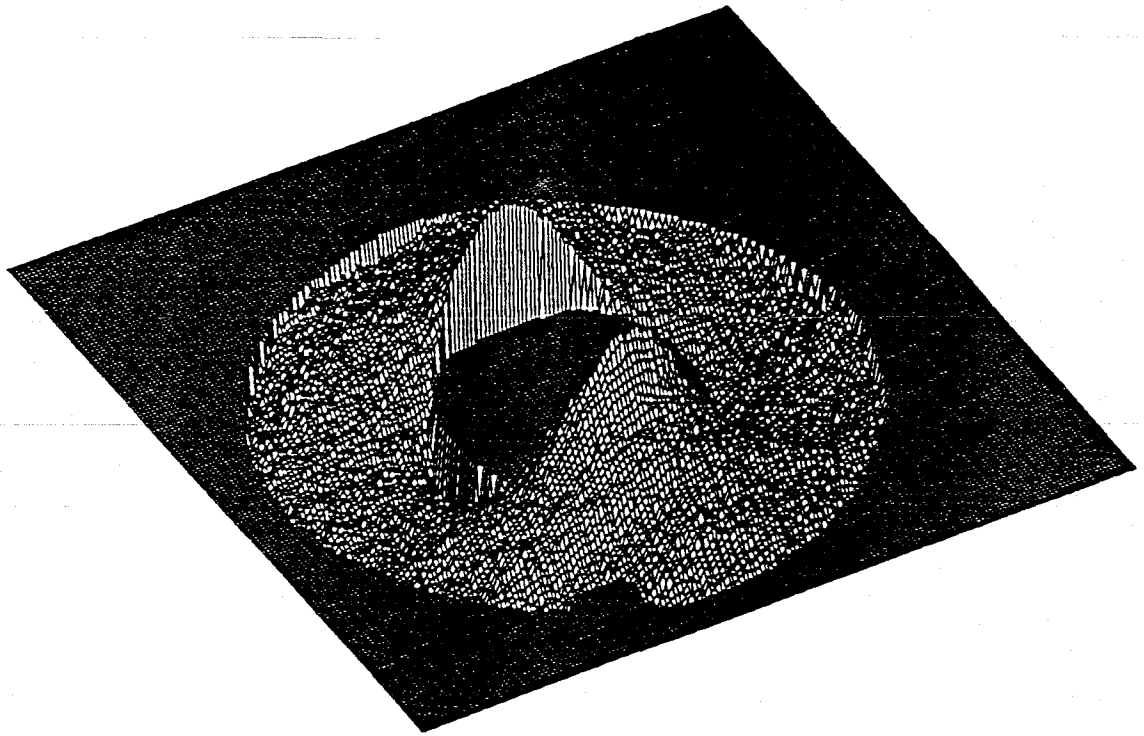
Figure 12. The difference of the horizontally polarized phasefront and the
vertically polarized phasefront for the 3.5 inch test piece.
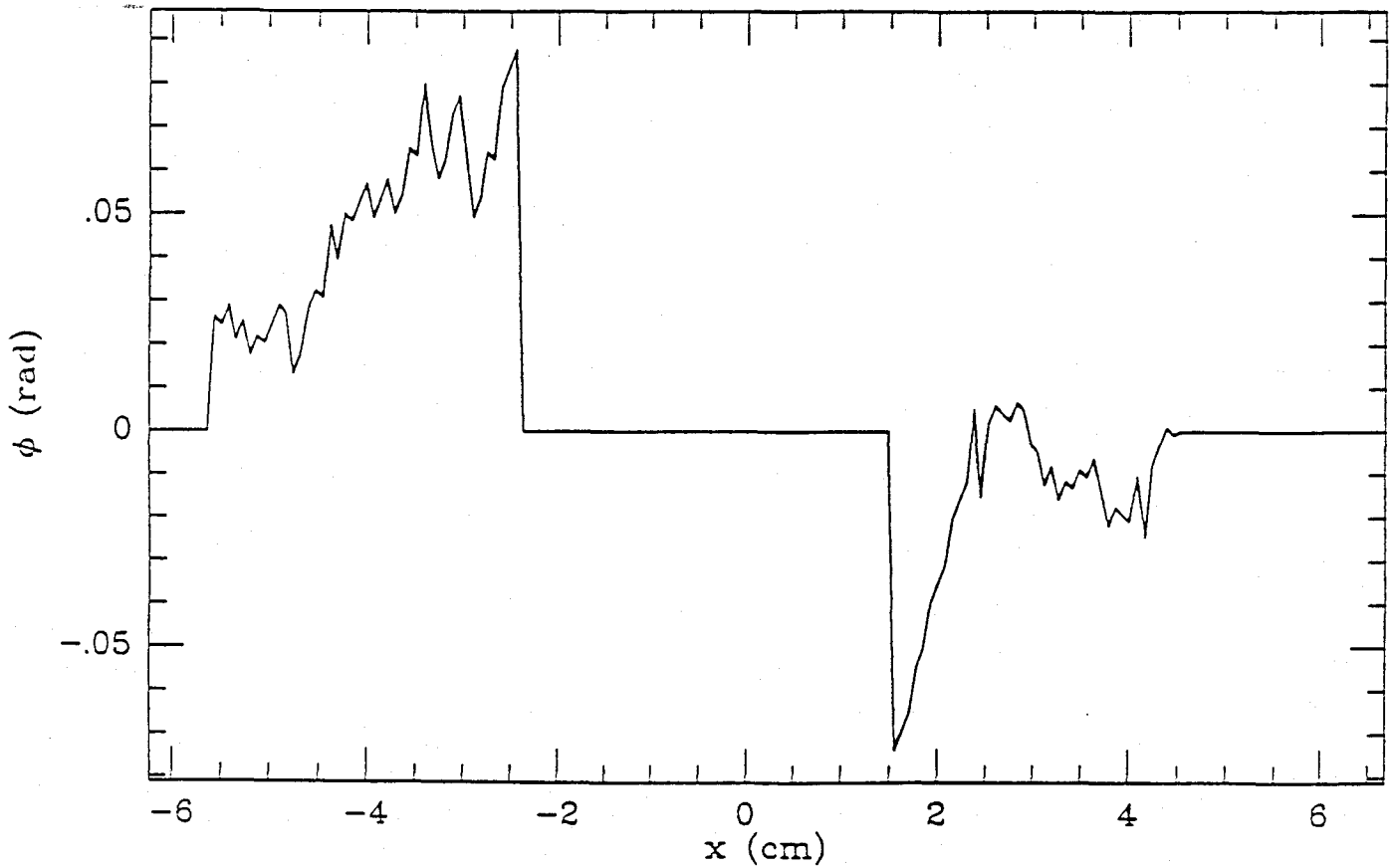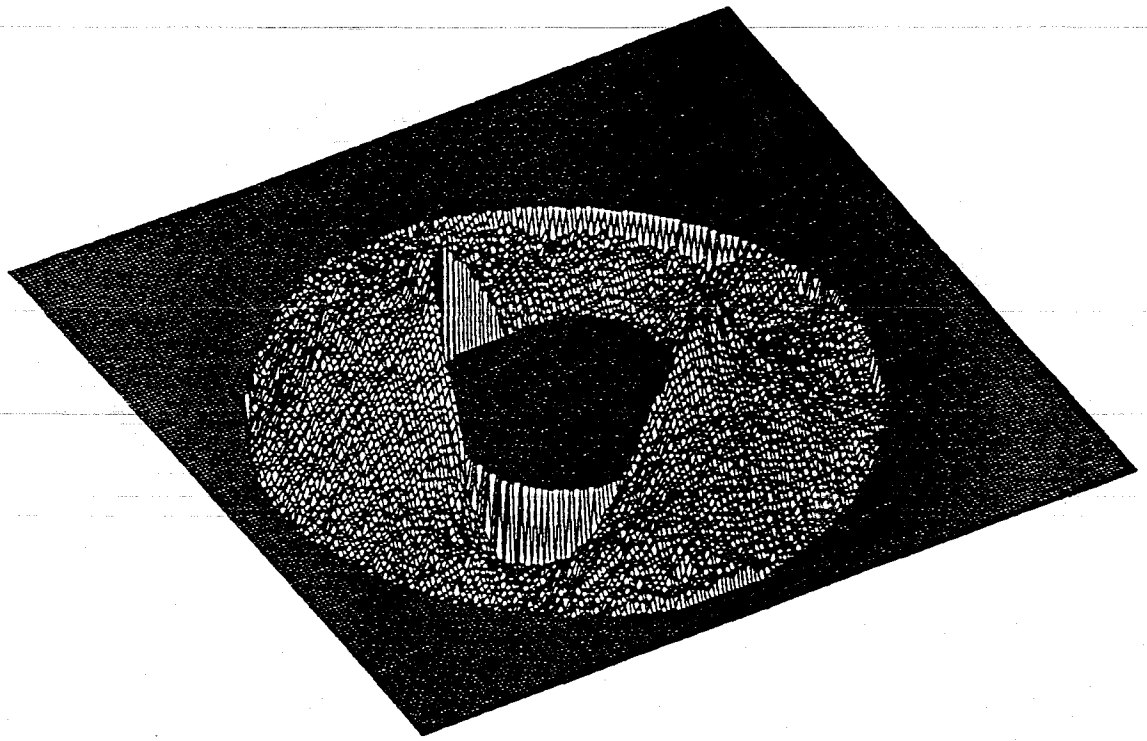
Figure 13. The difference of two phasefronts; one polarized at 45 degrees, the other at 135 degrees from the vertical, for the 3.5 inch test piece.
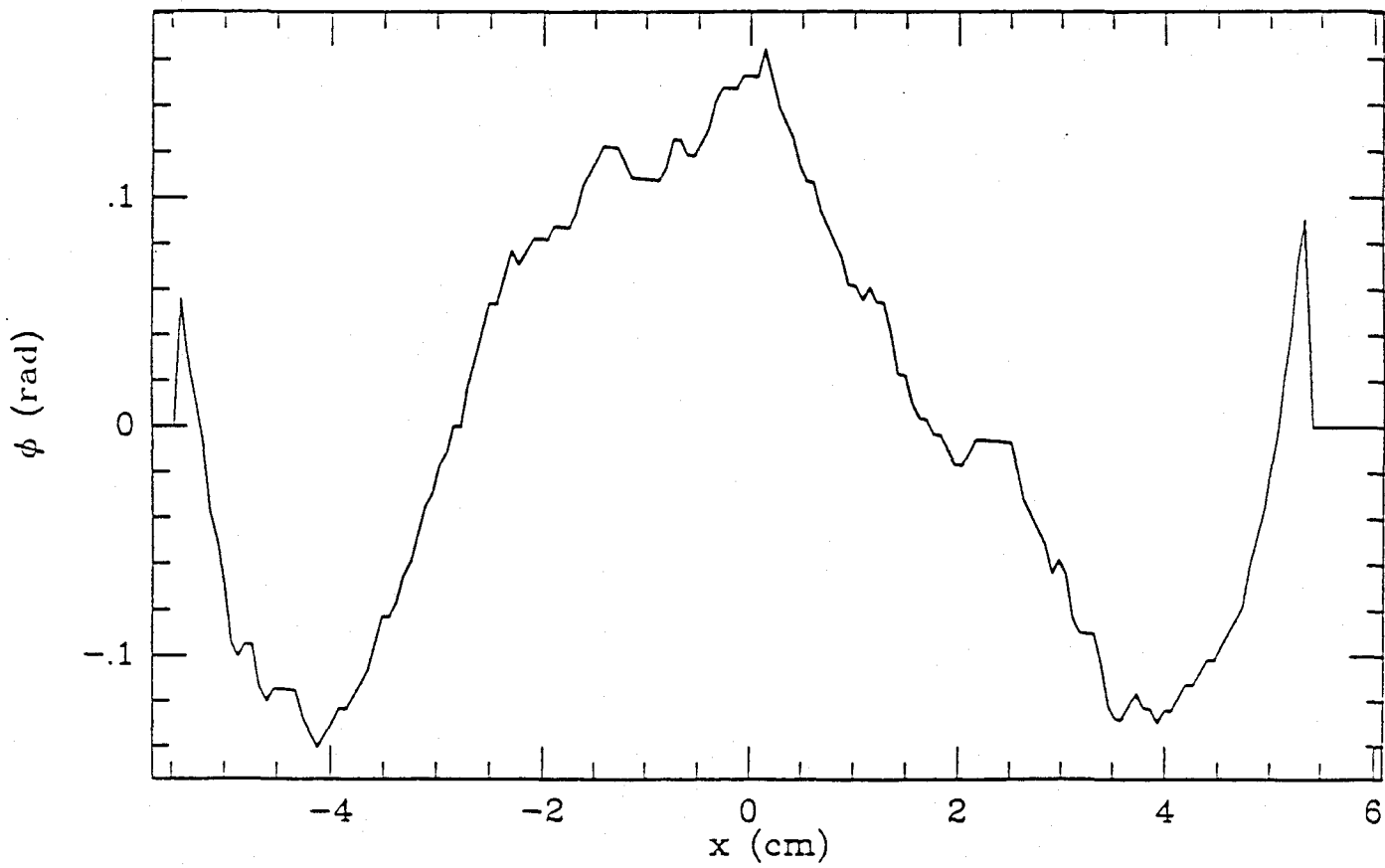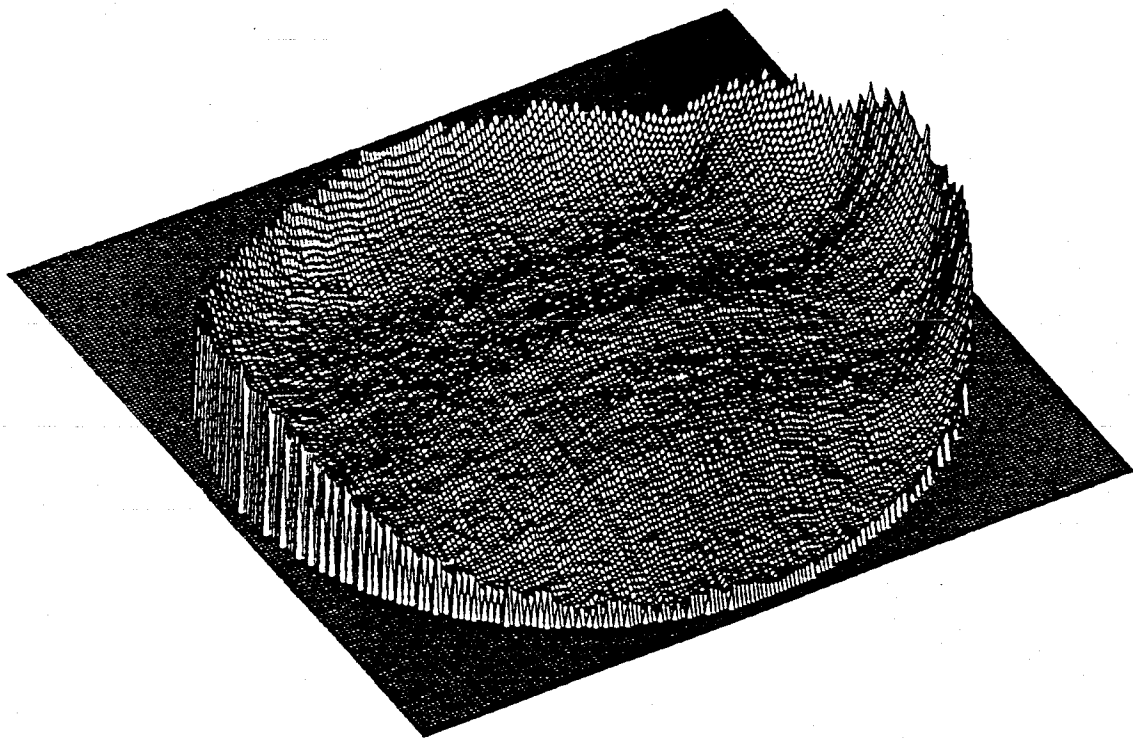
Figure 14.   The 1.5 inch test piece in vertically polarized light.
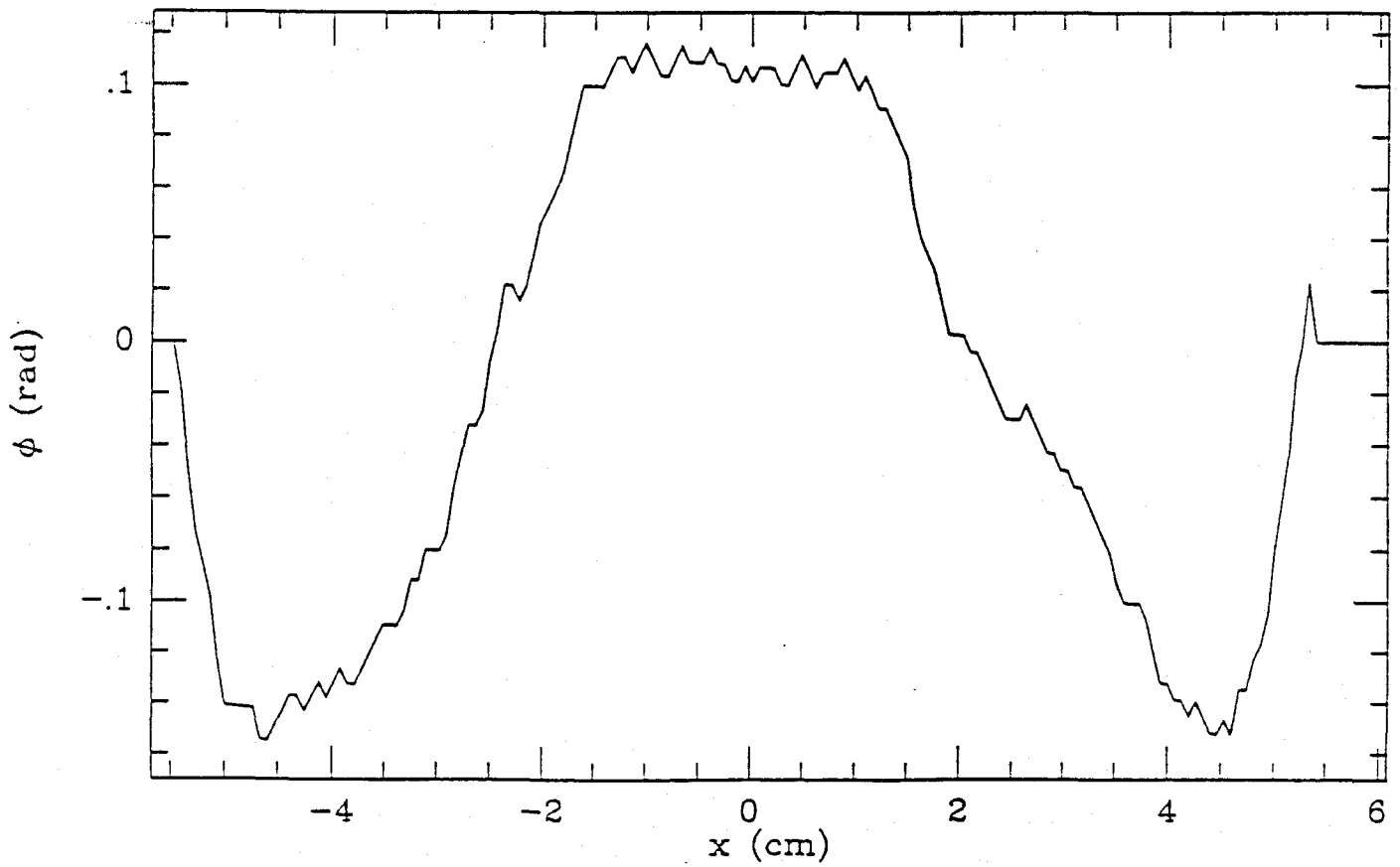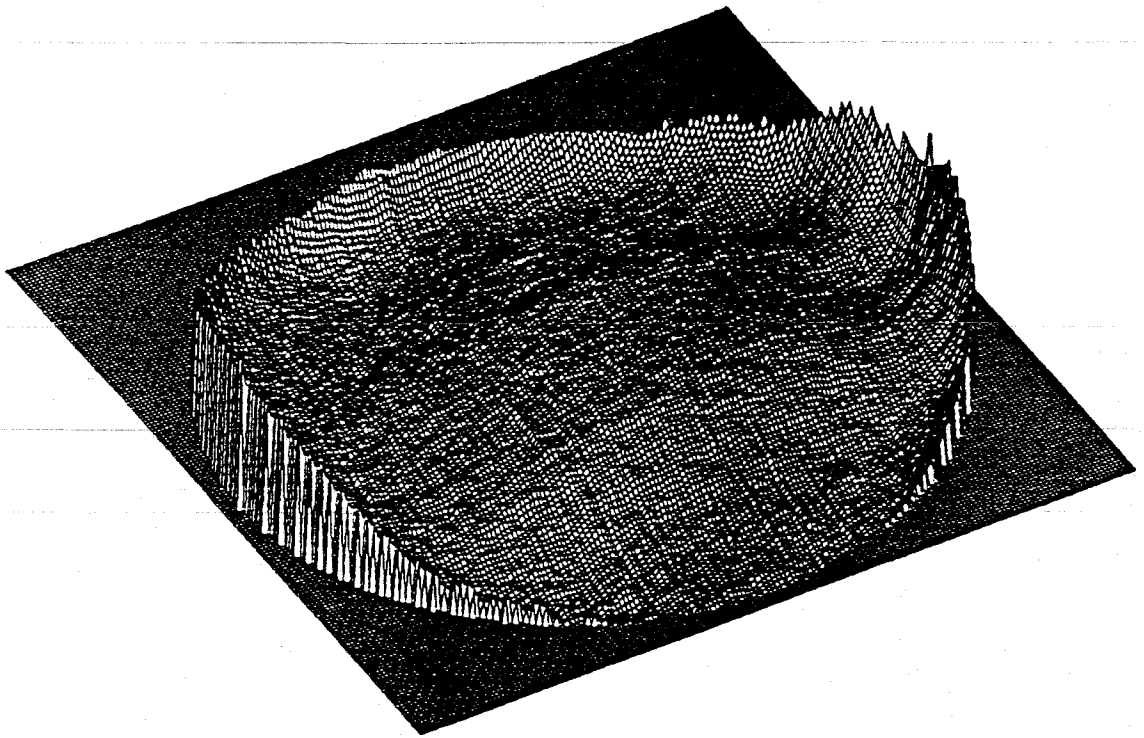
Figure 15.   The 1.5 inch test piece in horizontally polarized light.

WFO−WFQ
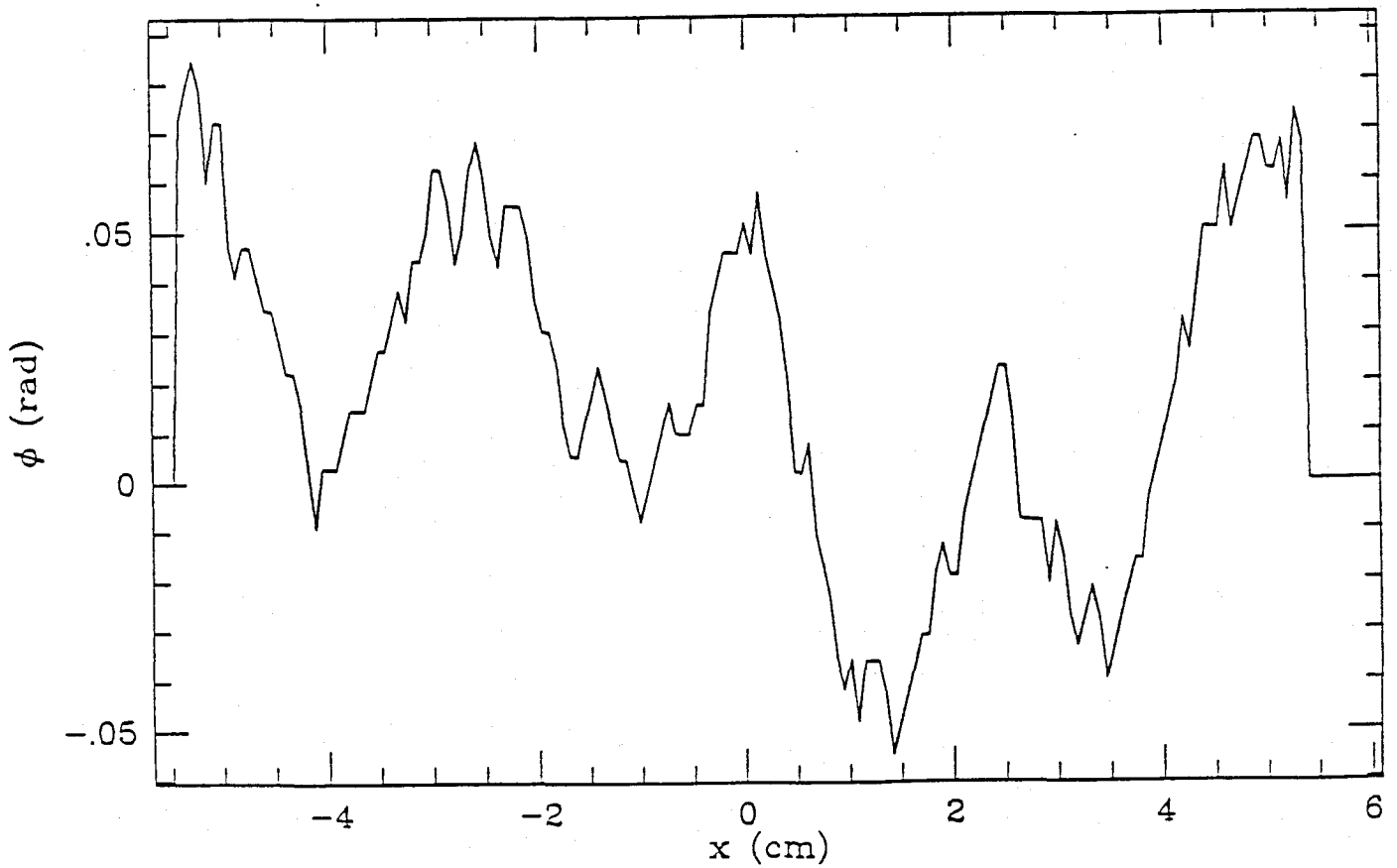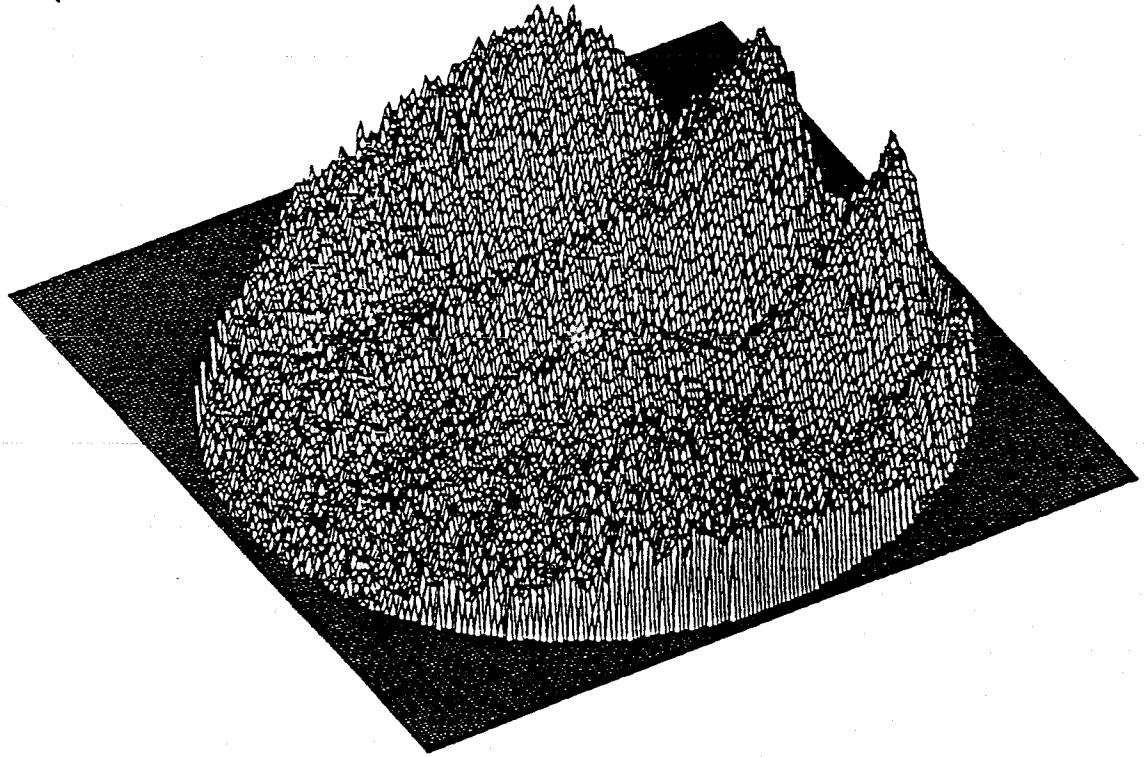
Figure 16. The difference of the horizontally polarized and the vertically
polarized phasefronts of the 1.5 inch test piece.
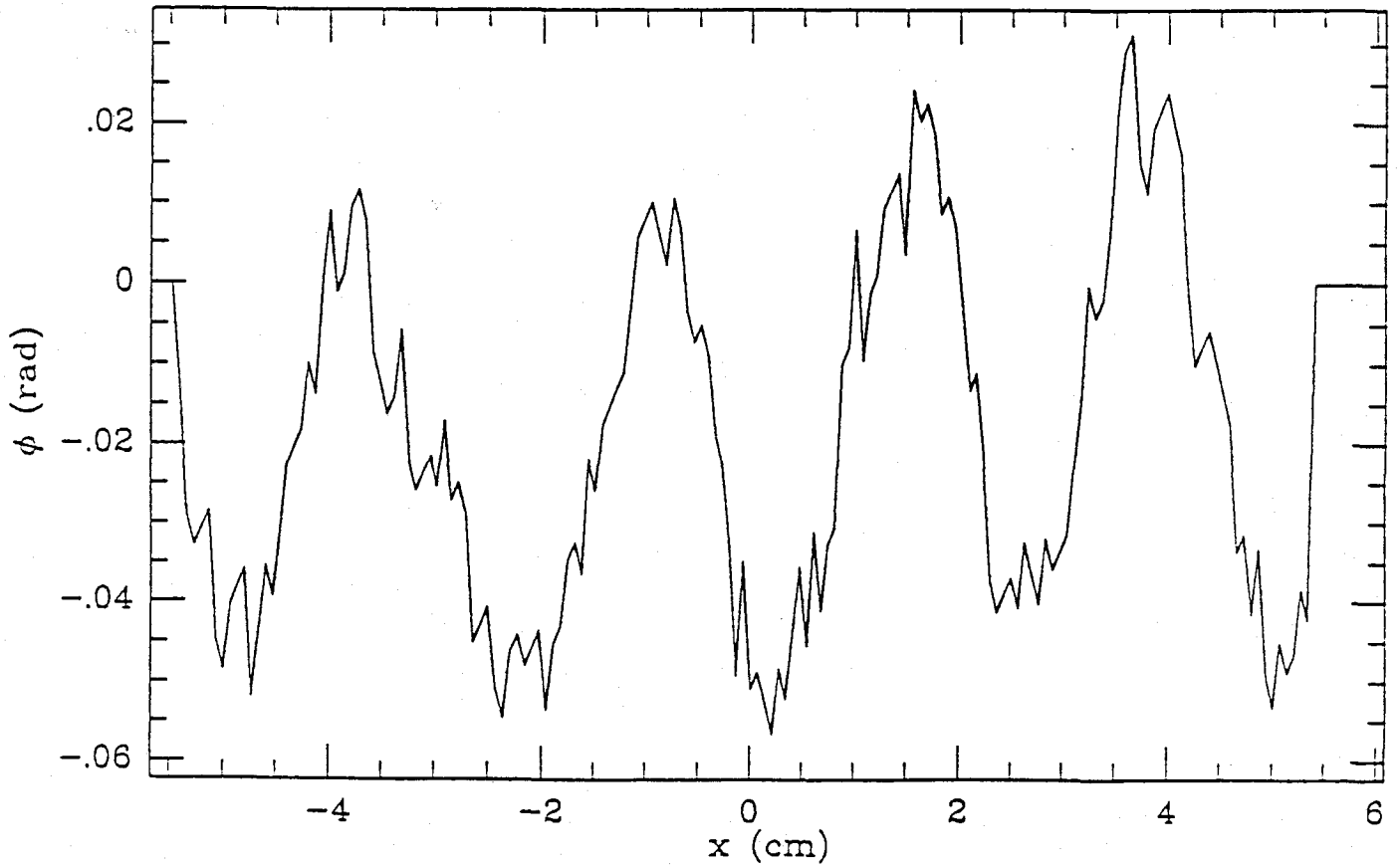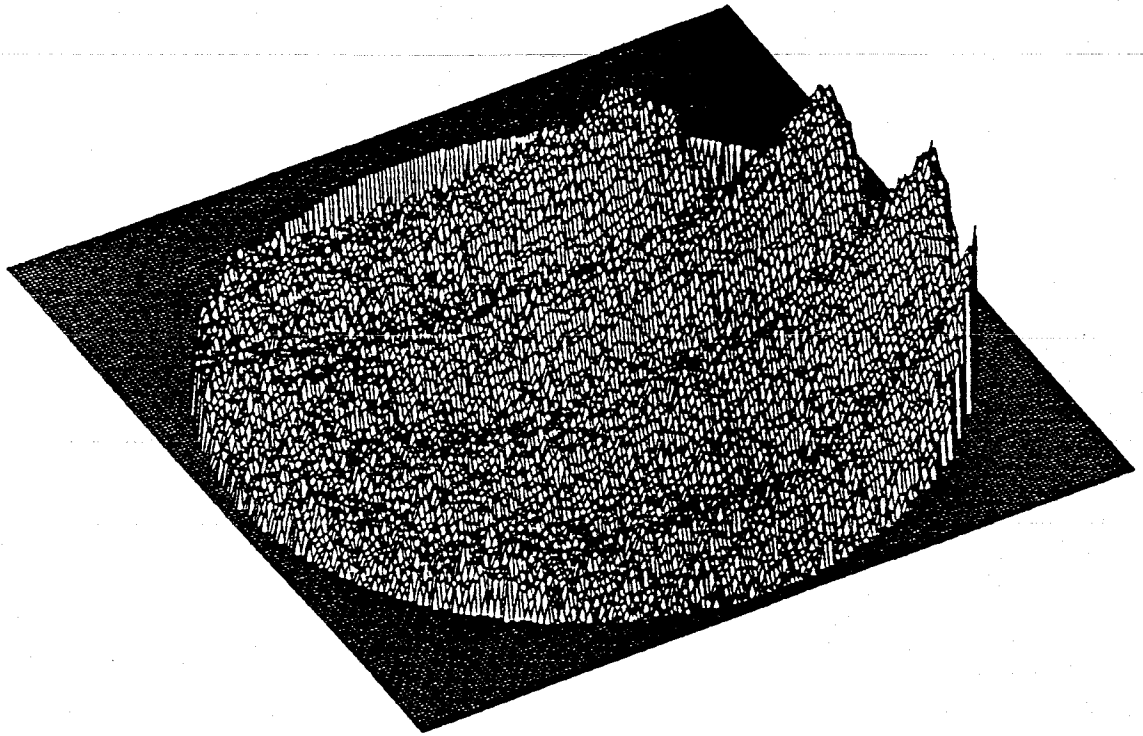
Figure 17.   The difference of the 1.5 inch test piece phasefronts in light
             polarized at 45 degrees and 135 degrees from the vertical.

Autocovariance

$\delta=1.03E-02$ rad^2

$\alpha=2.08$ cm

Row 48

$\delta=5.36E-03$ rad^2

$\alpha=2.60$ cm

Row 115

$\delta=1.80E-03$ rad^2

$\alpha=1.04$ cm

Column 48

$\delta=5.78E-03$ rad^2

$\alpha=1.78$ cm

Column 115
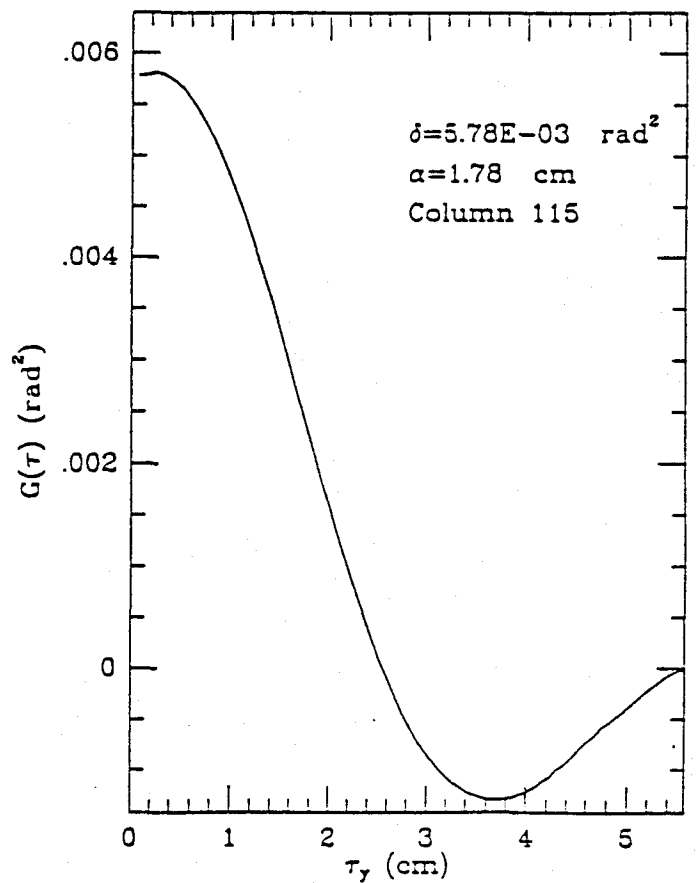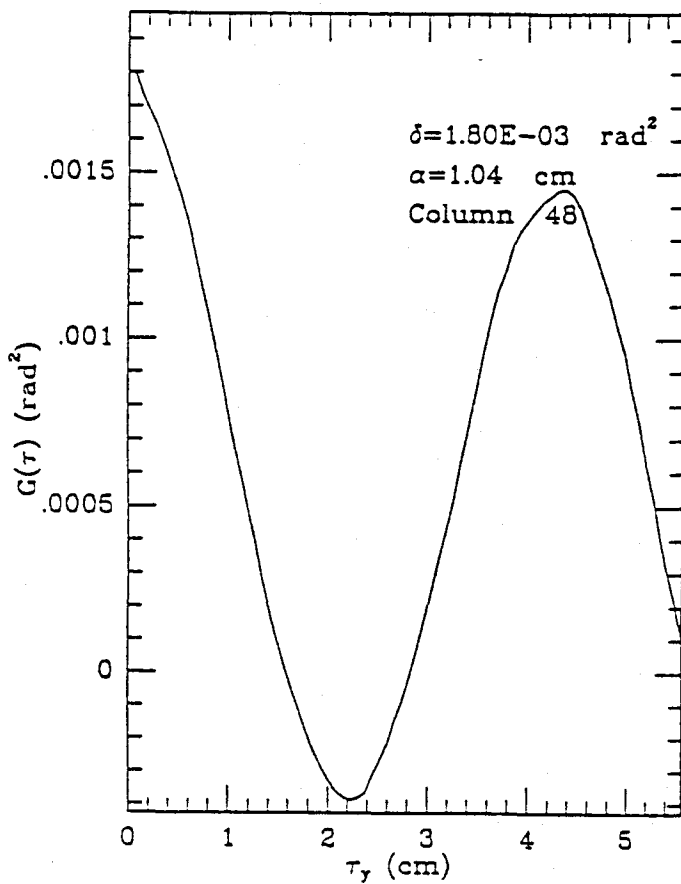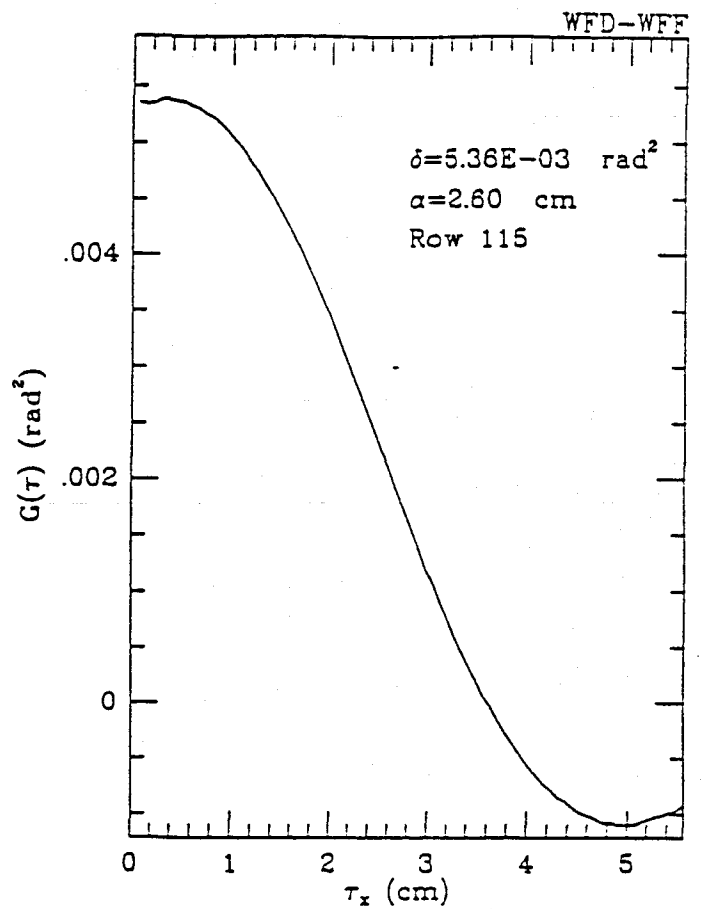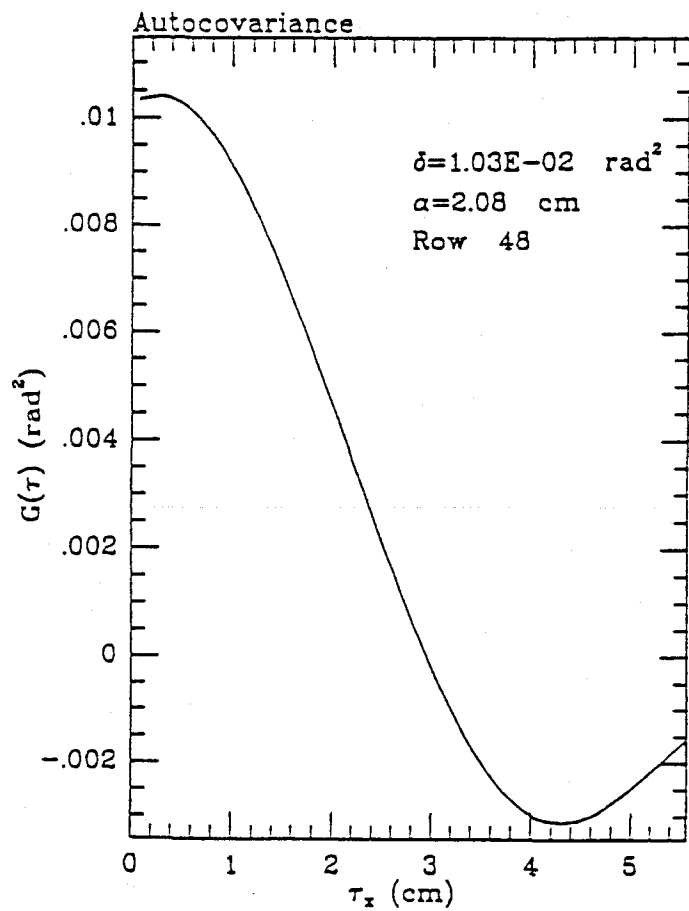
Figure 18.   Autocovariance functions of the horizontal/vertical difference
phasefronts of the 3.5 inch test piece.
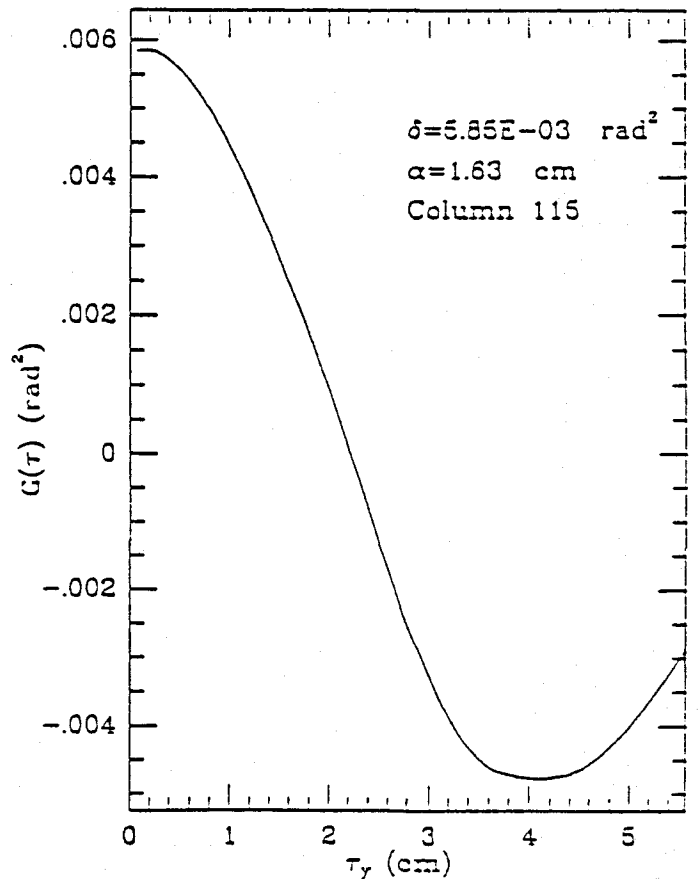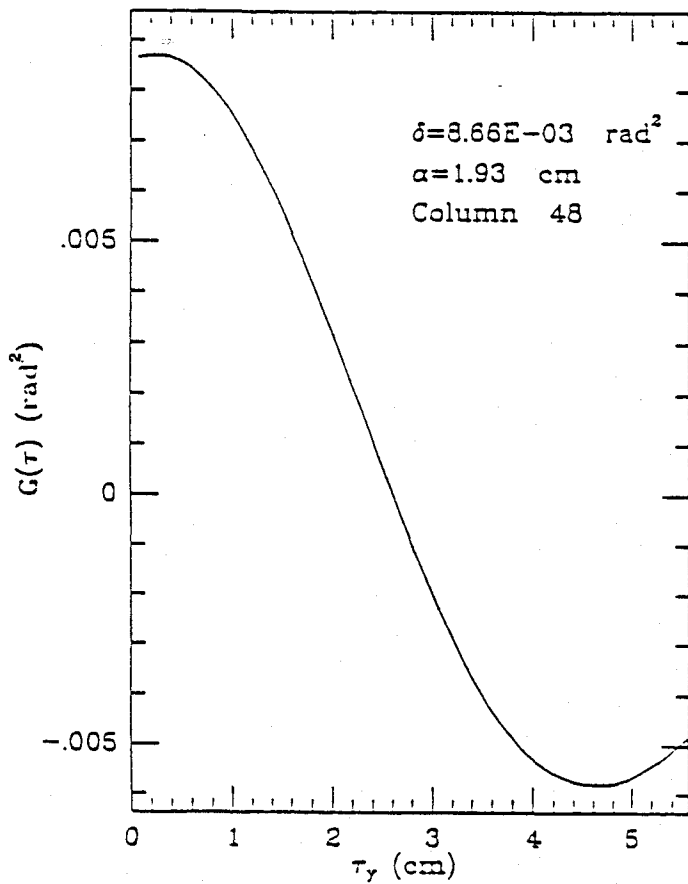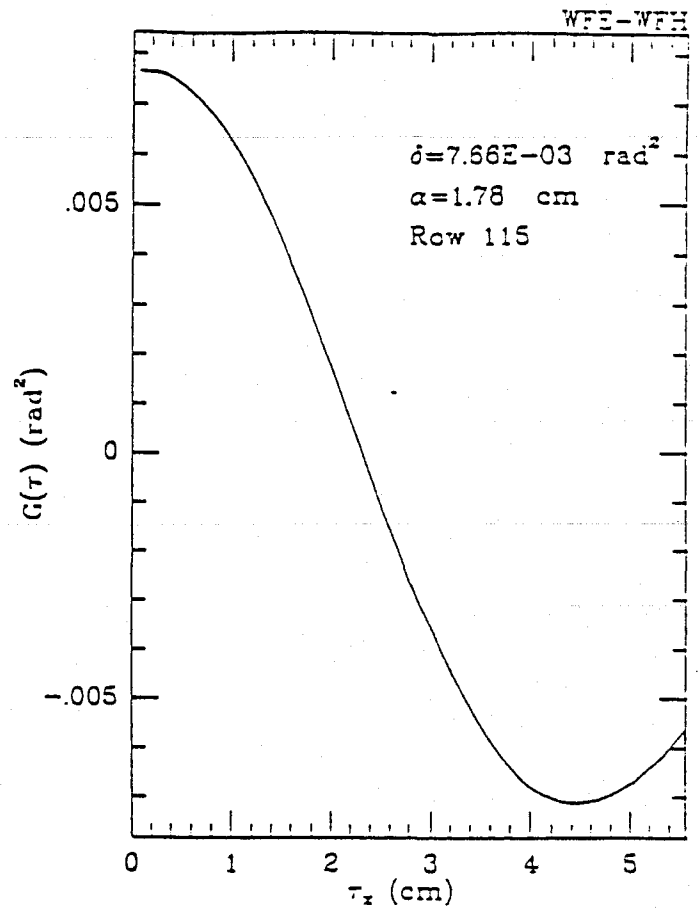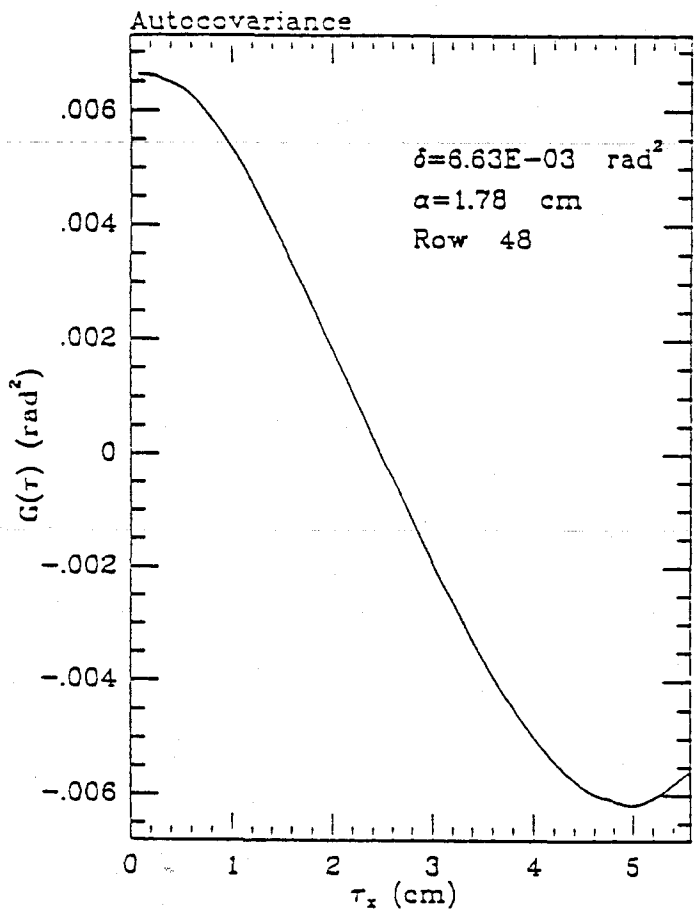
Figure 19. Autocovariance functions of the 45/135 degree difference phasefronts of the 3.5 inch test piece.
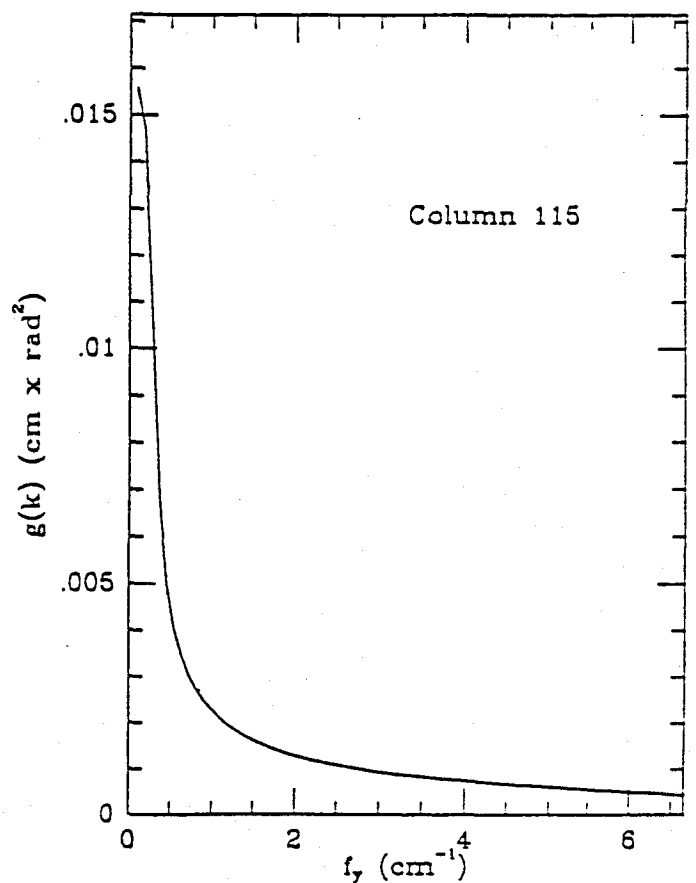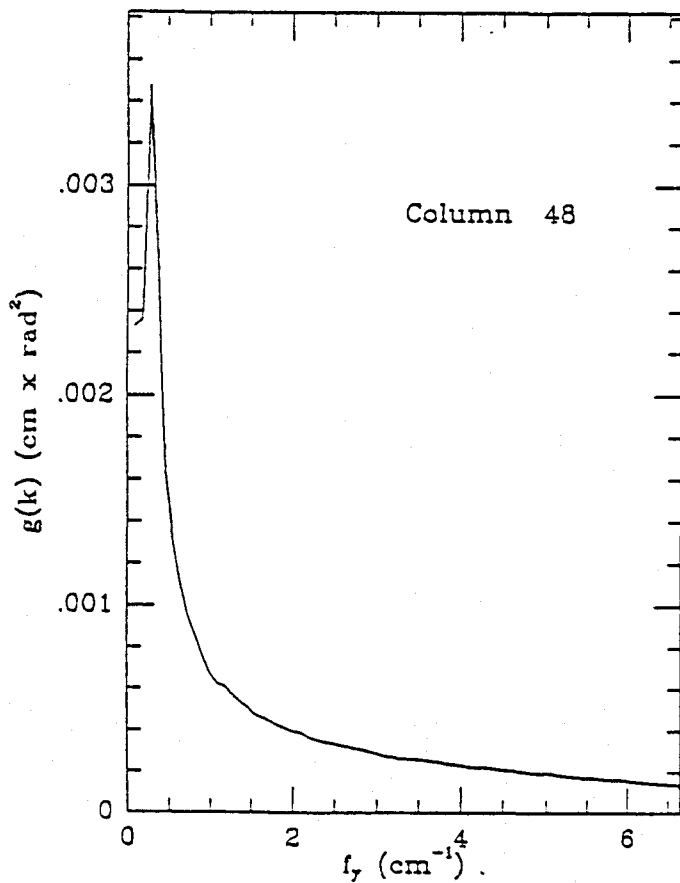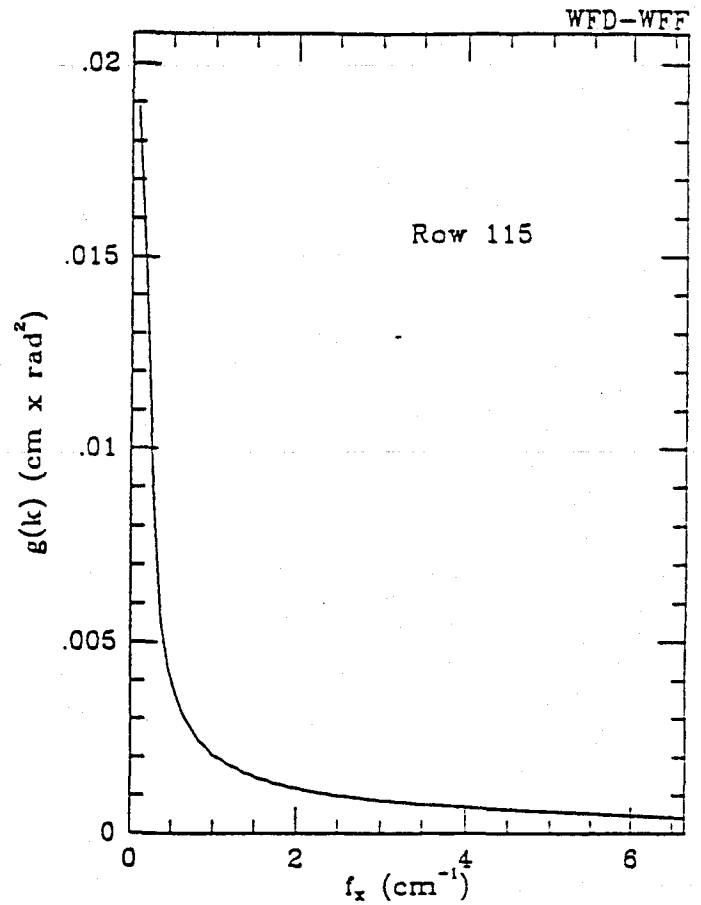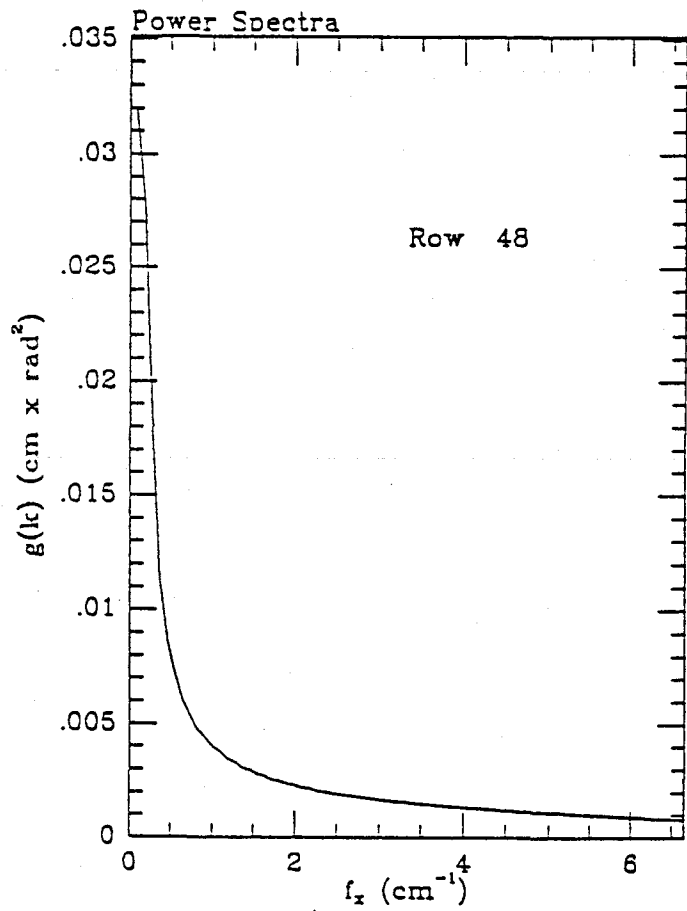
Figure 20.   Fourier transforms of the autocovariance functions of the
             horizontal/vertical difference phasefronts of the 3.5 inch
             test piece.
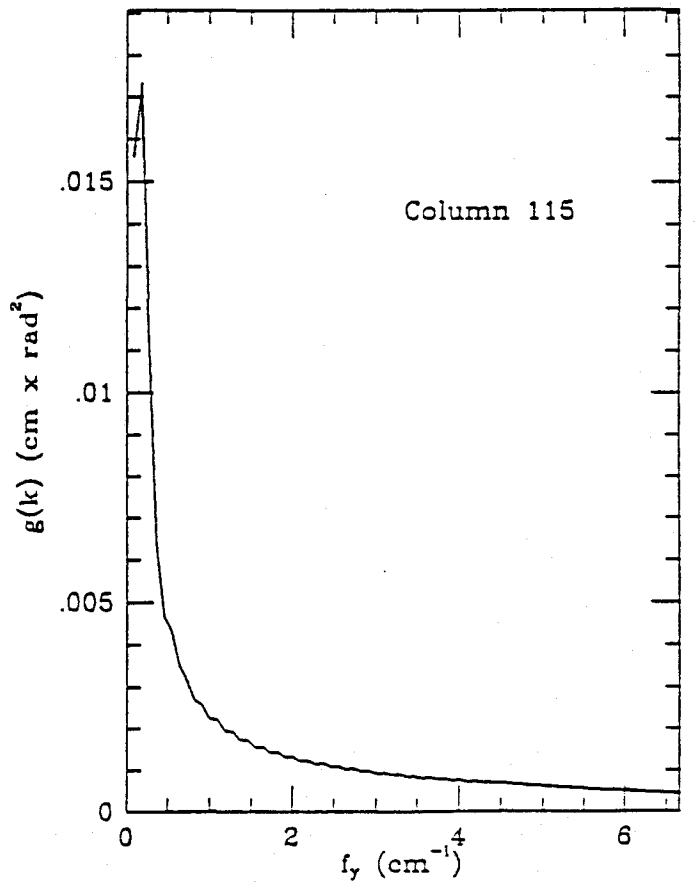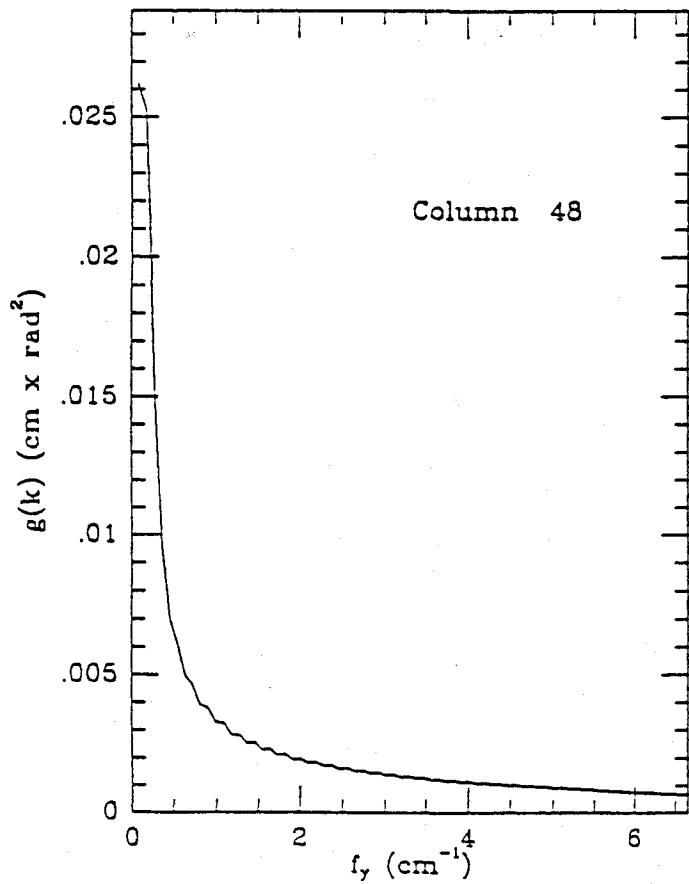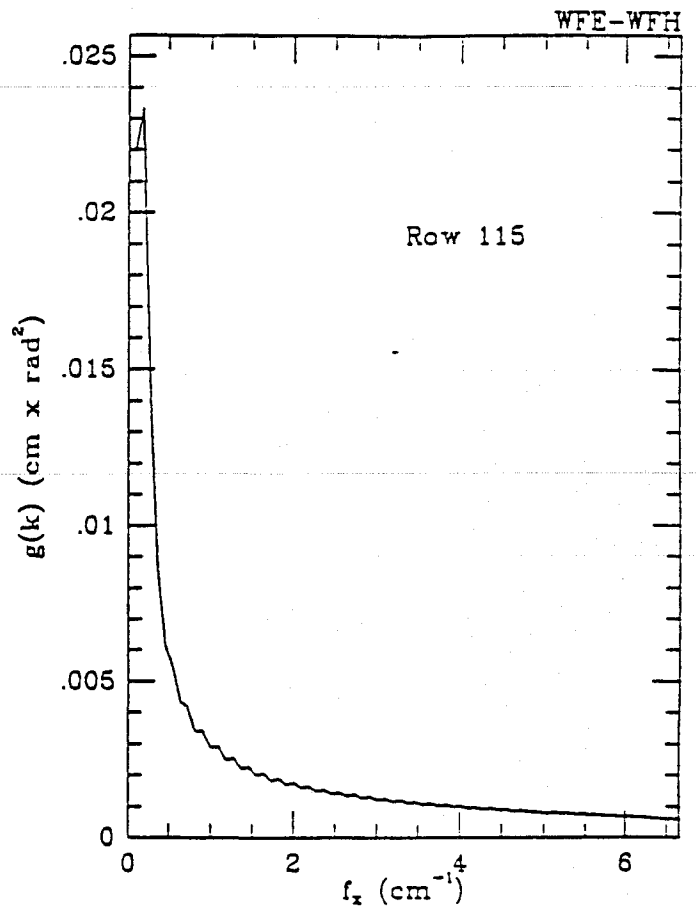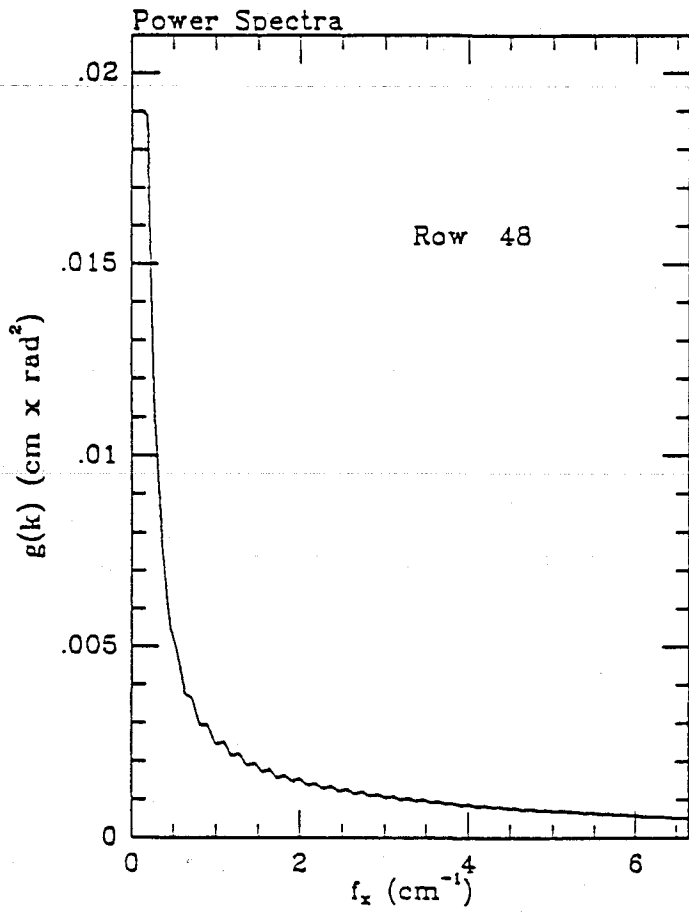
Figure 21.   Fourier transforms of the autocovariance functions of the
             45/135 degree difference phasefronts of the 3.5 inch test piece.

δ=1.48E-03 rad^2
α=4.19 cm
Row 48

$G(\tau)$ (rad^2)

τ_x (cm)

δ=8.21E-04 rad^2
α=1.01 cm
Row 115

$G(\tau)$ (rad^2)

τ_x (cm)

δ=5.51E-04 rad^2
α=2.03 cm
Column 48

$G(\tau)$ (rad^2)

τ_y (cm)

δ=2.11E-03 rad^2
α=0.61 cm
Column 115

$G(\tau)$ (rad^2)

τ_y (cm)
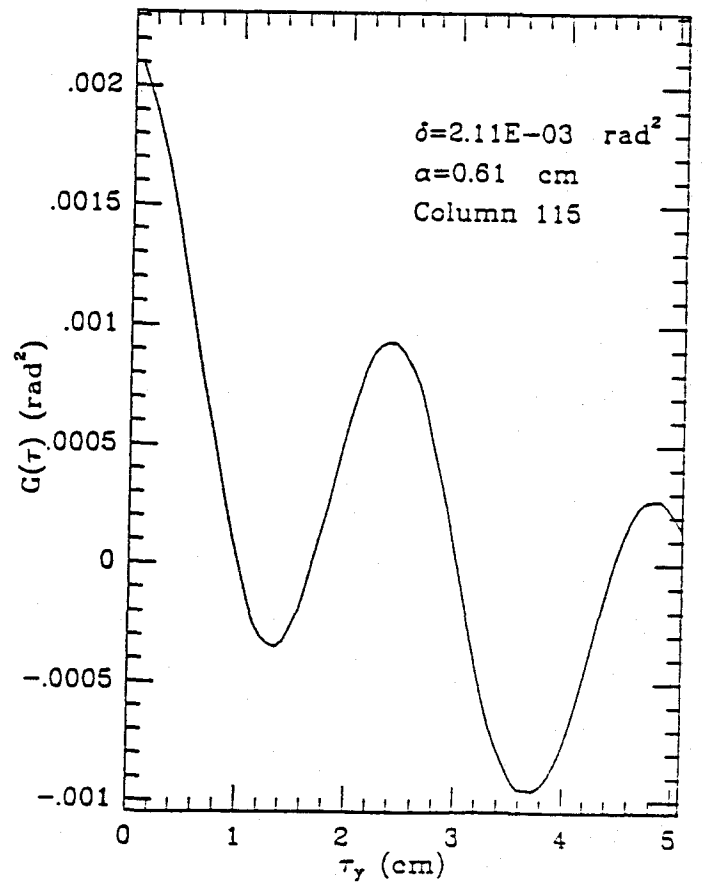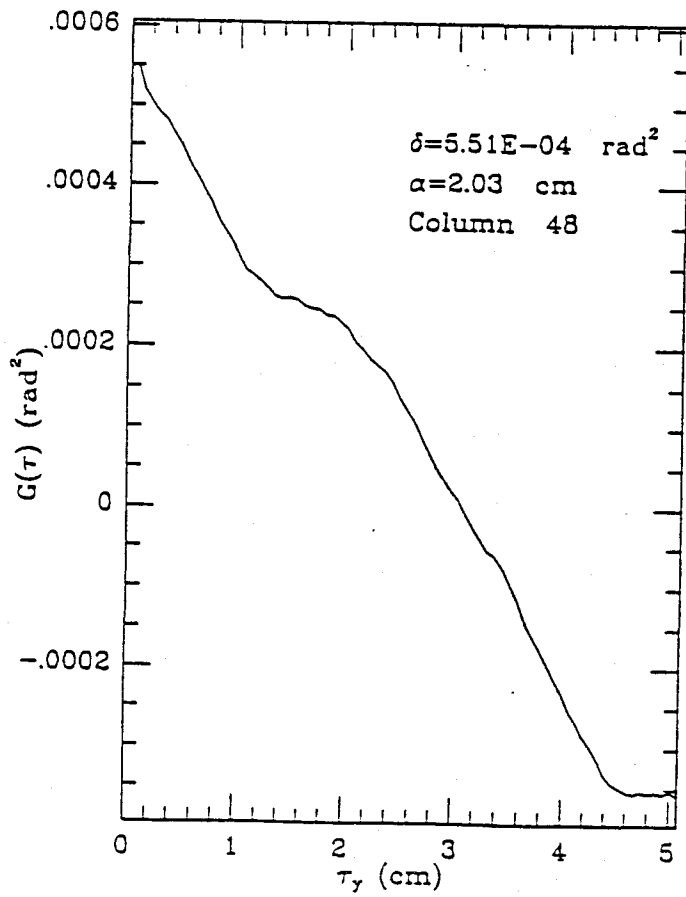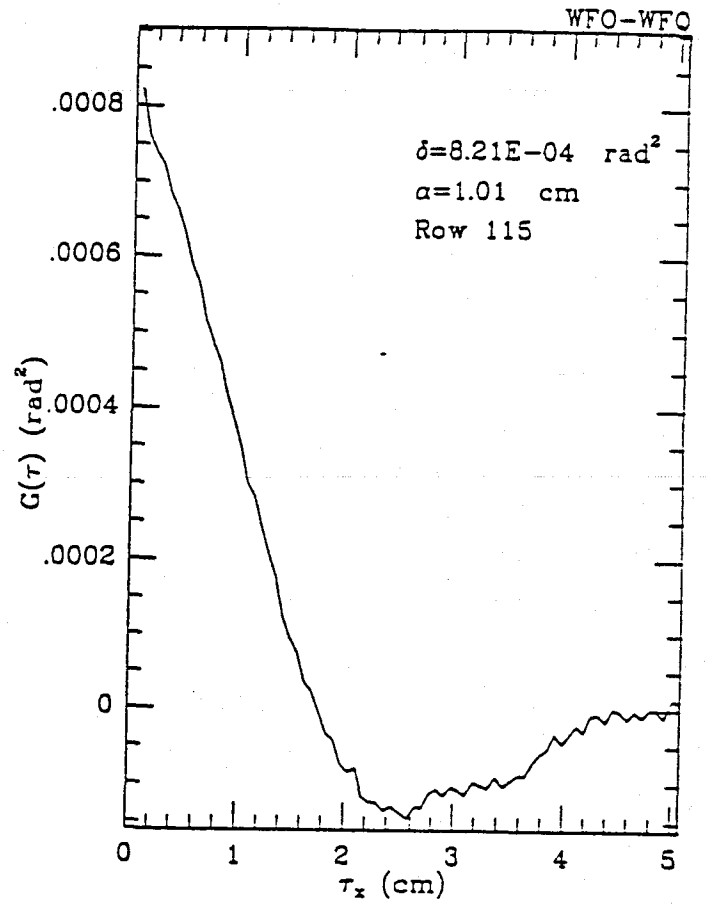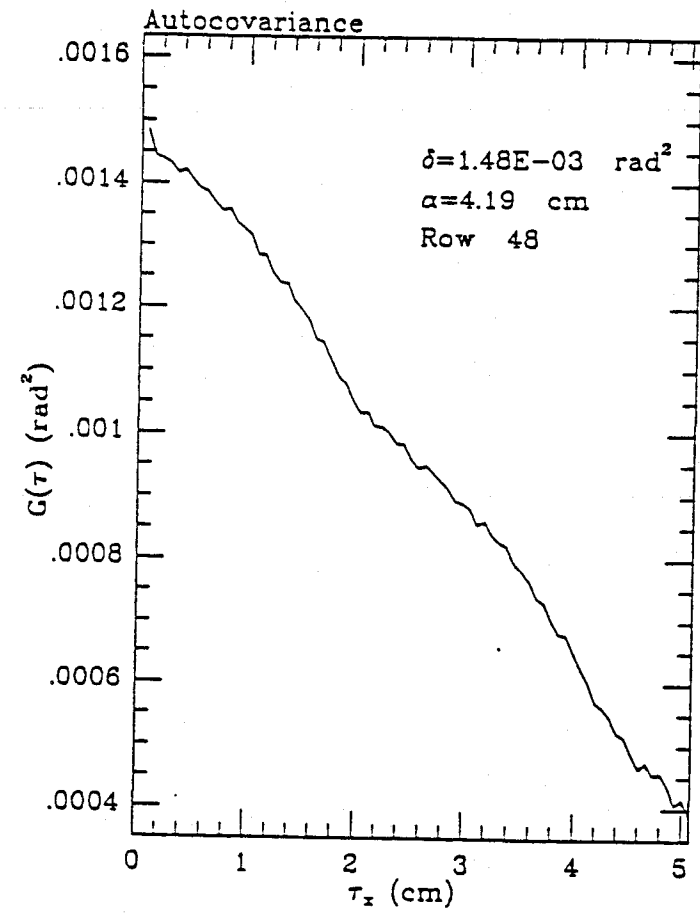
Figure 22. Autocovariance functions of the horizontal/vertical polarization
difference phasefronts of the 1.5 inch test piece.
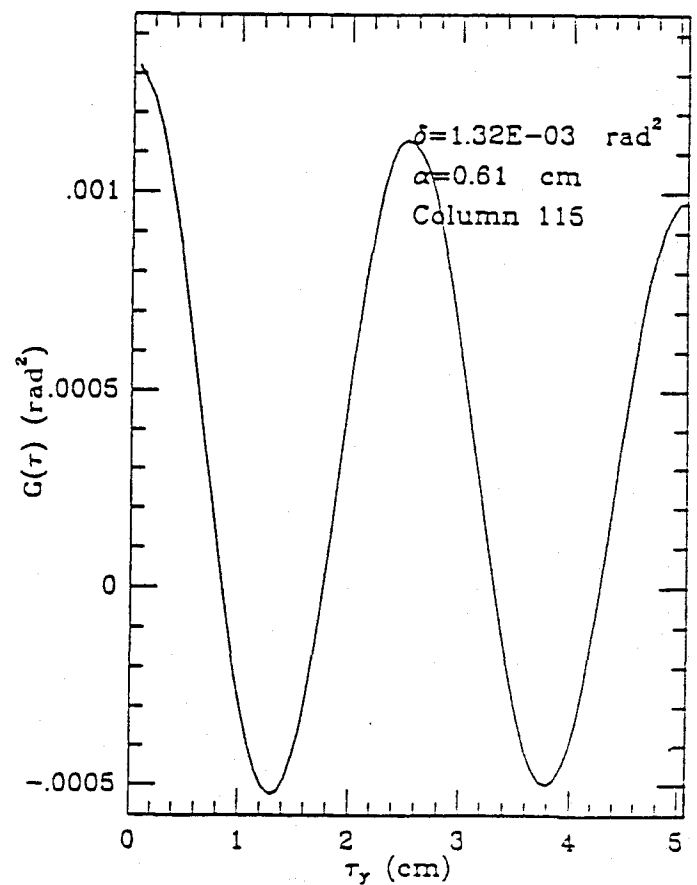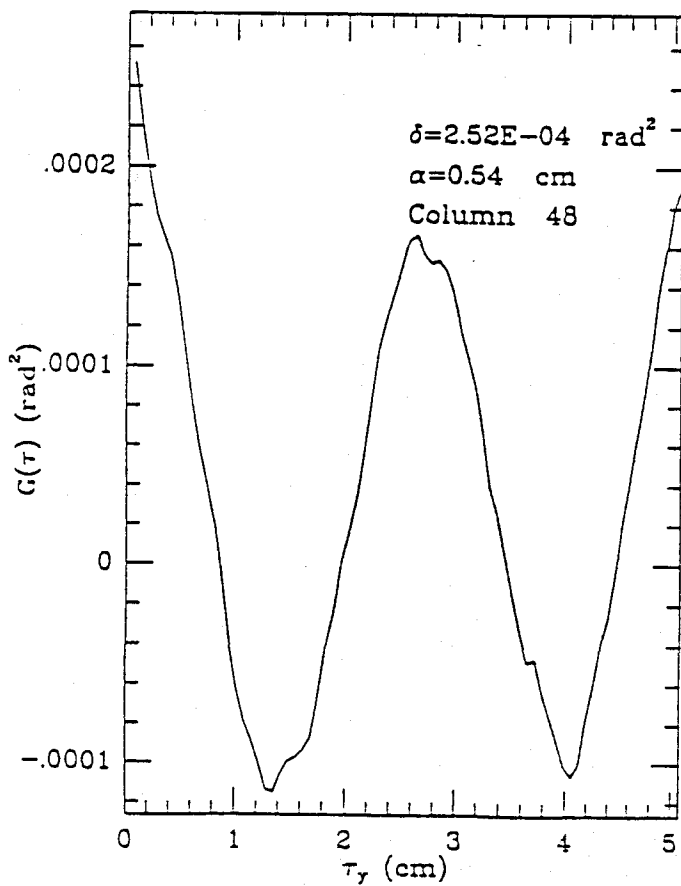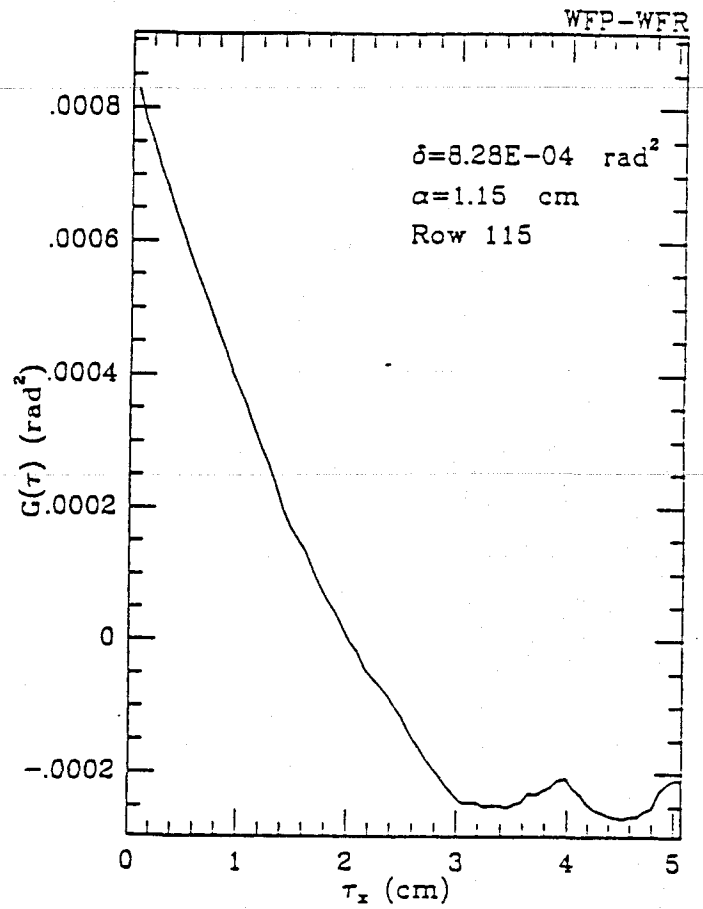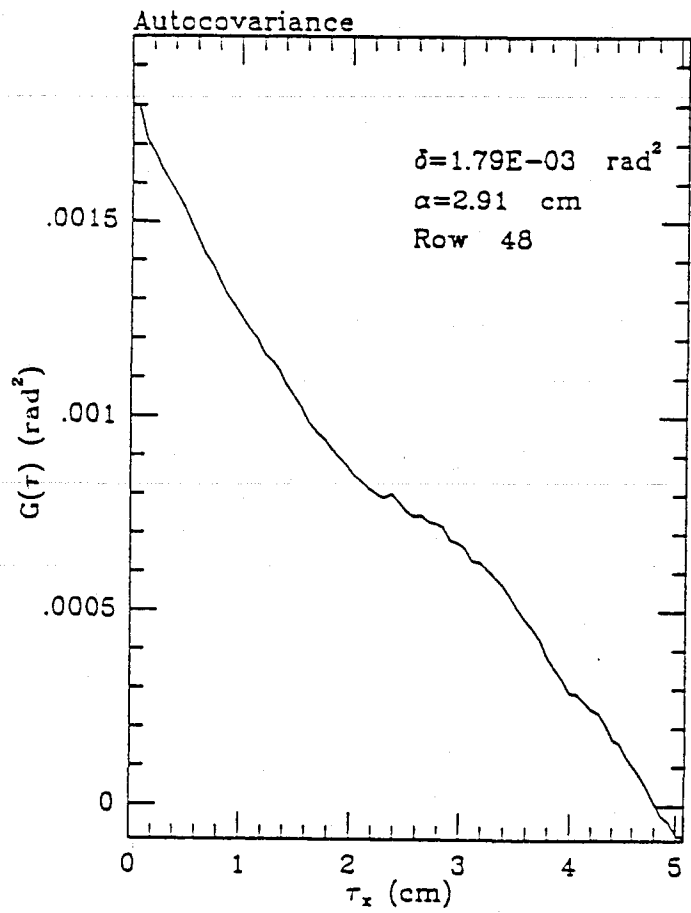
Figure 23. Autocovariance functions of the 45/135 degree polarization difference phasefronts of the 1.5 inch test piece.
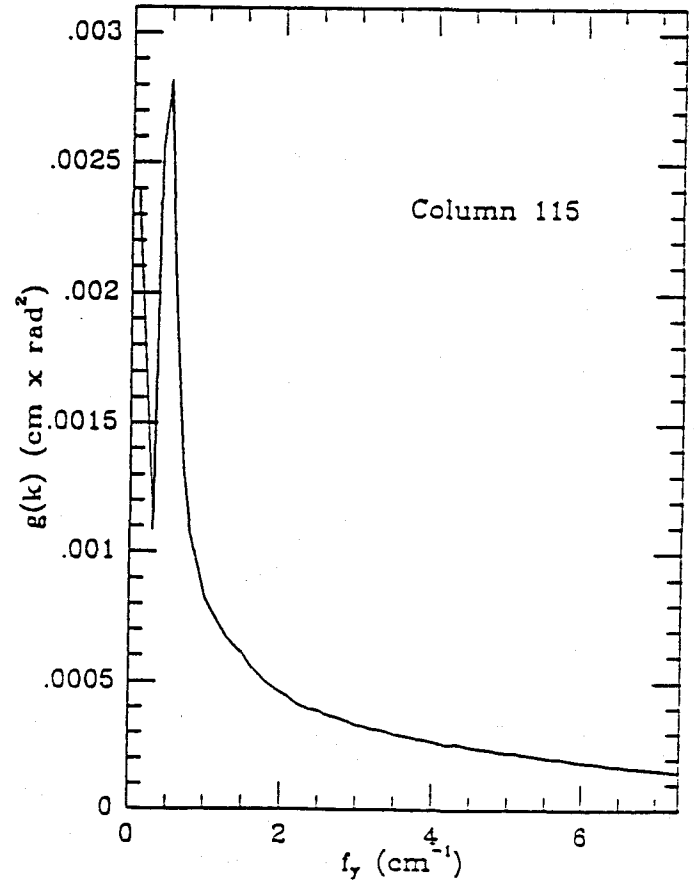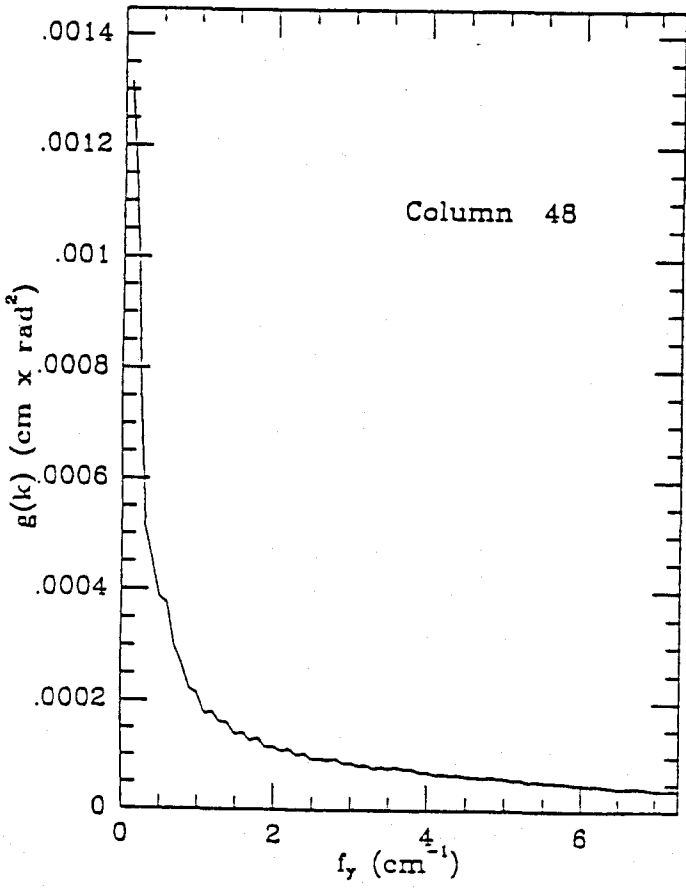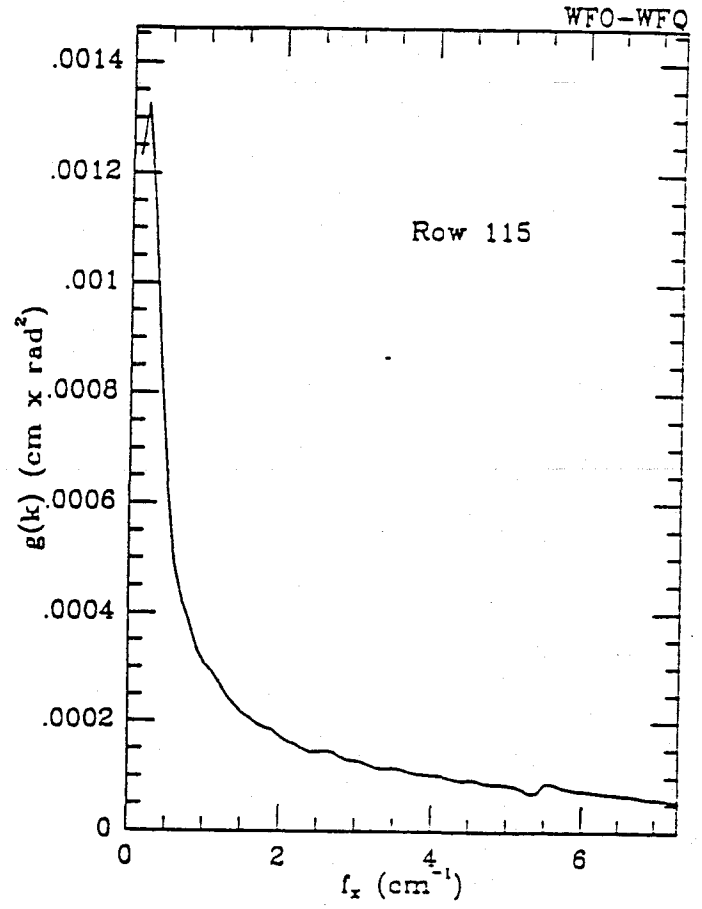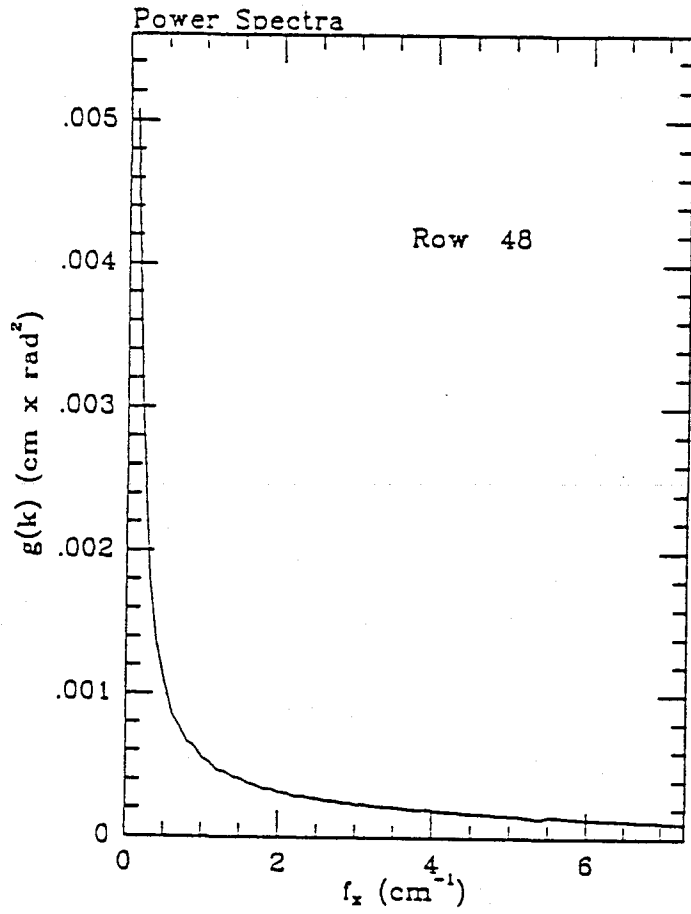
Figure 24. Fourier transforms of the autocovariance functions of the horizontal/vertical polarization difference phasefronts of the 1.5 inch test piece.
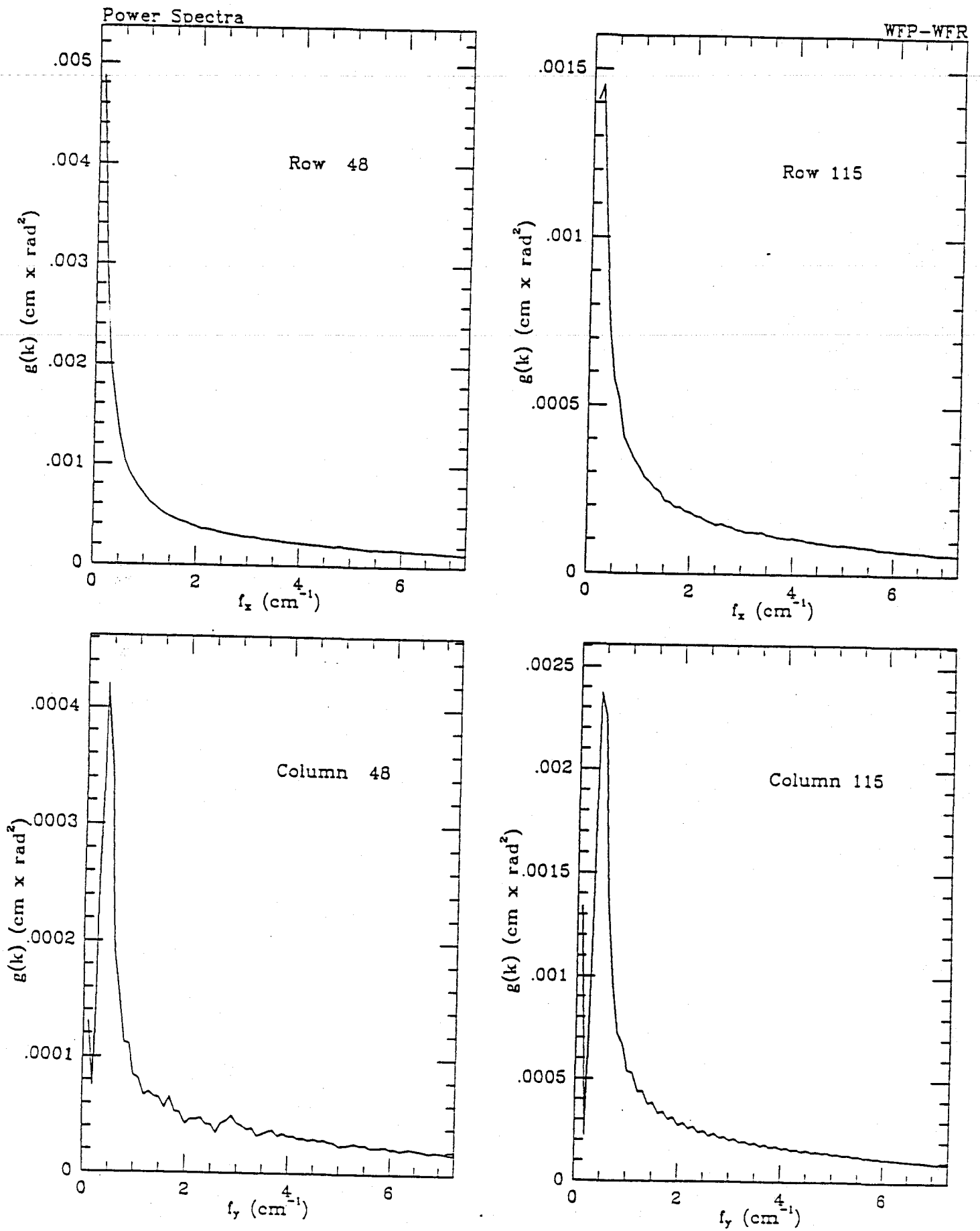
Figure 25. Fourier transforms of the autocovariance functions of the 45/135 degree polarization difference phasefronts of the 1.5 inch test piece.

3.5 Inch Piece
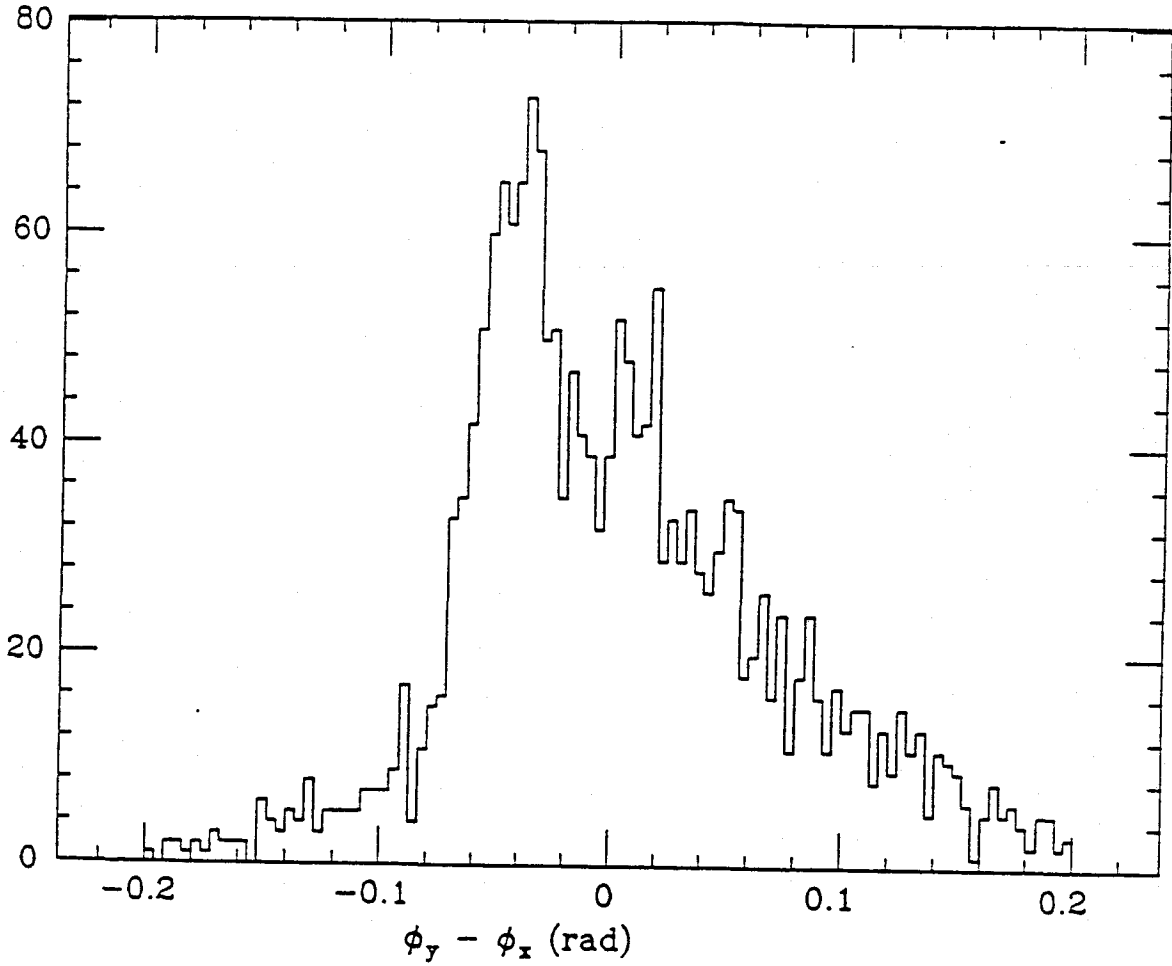
Figure 26.

1.5 Inch Piece

$\phi_y - \phi_x$ (rad)
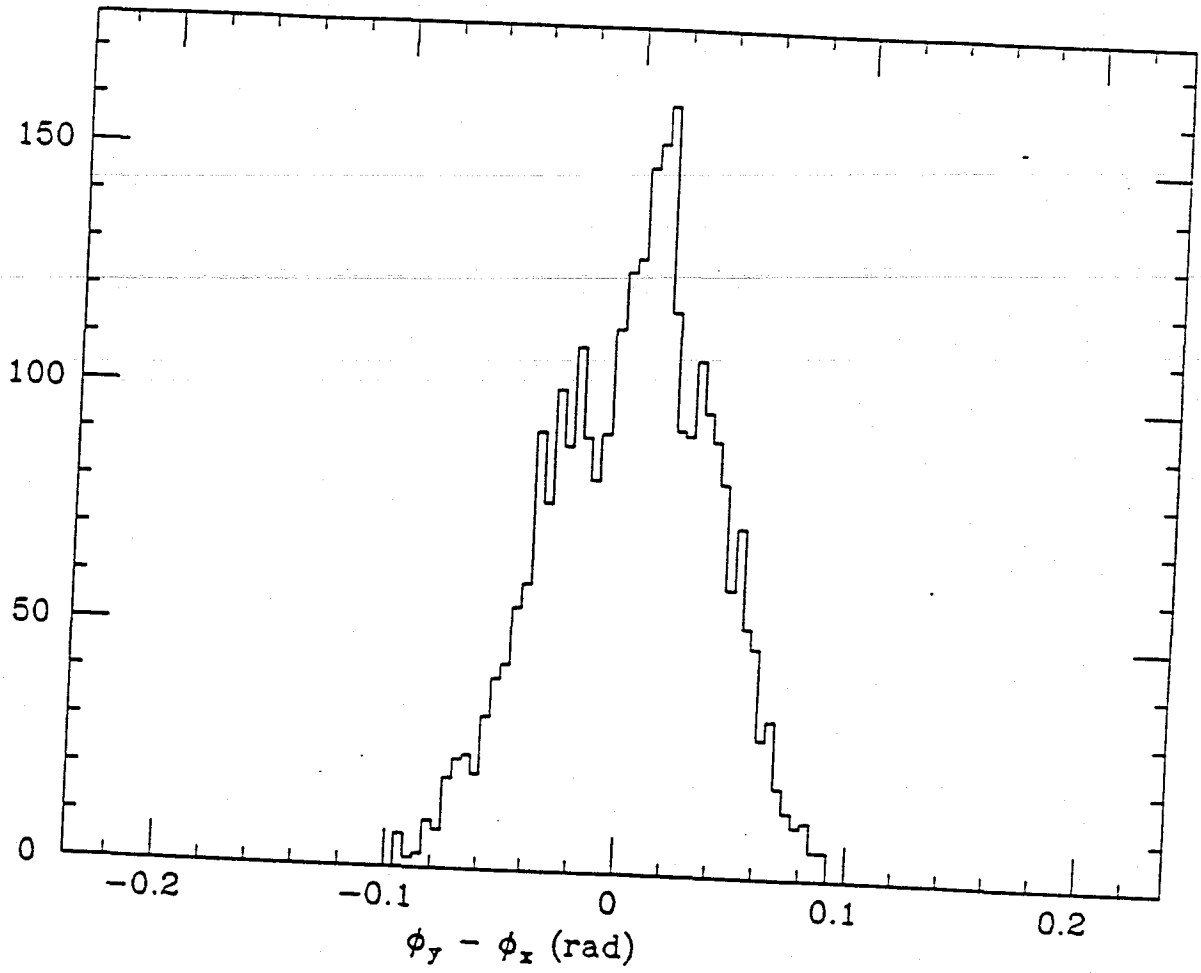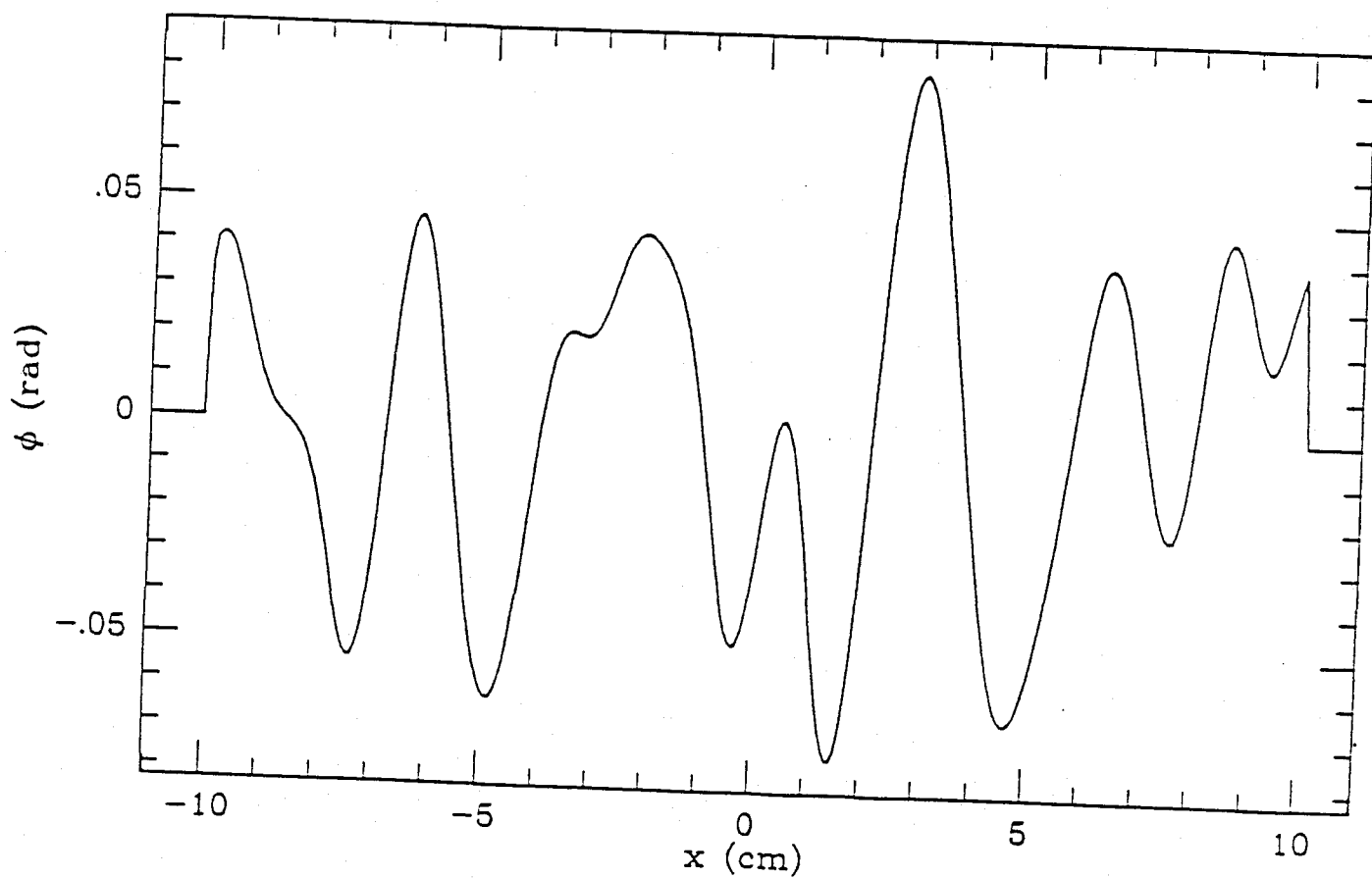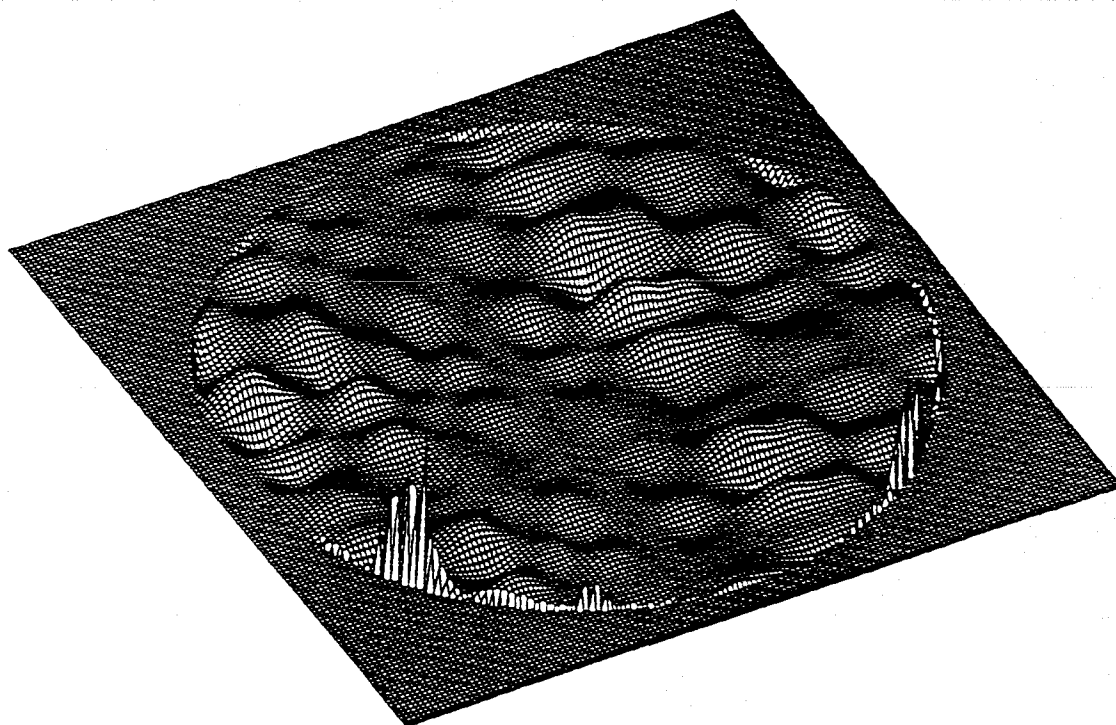
Figure 27.

Figure 28.   Phasefront generated from a computer simulation of fused silica blank.
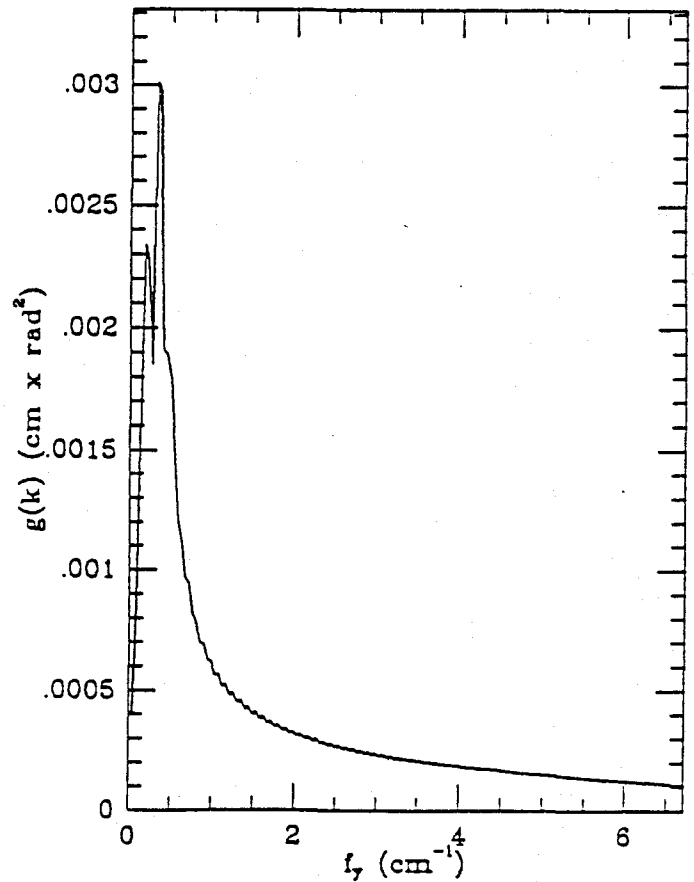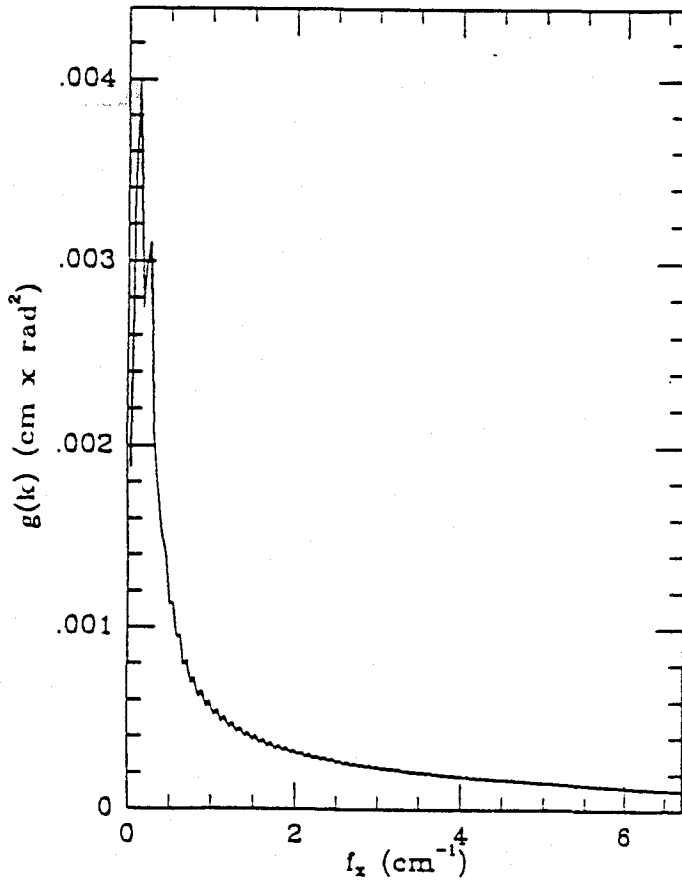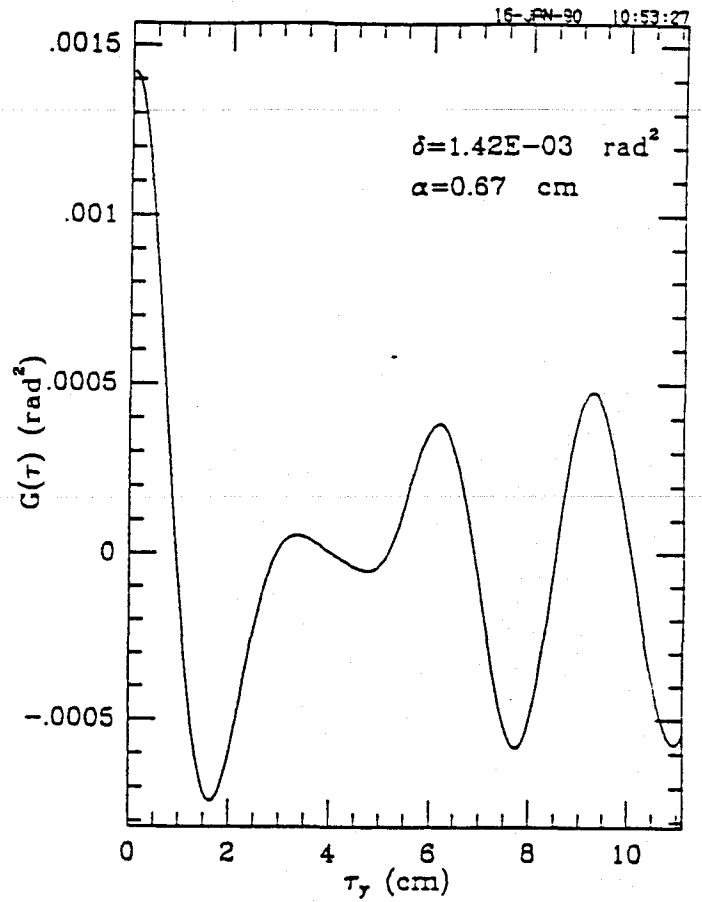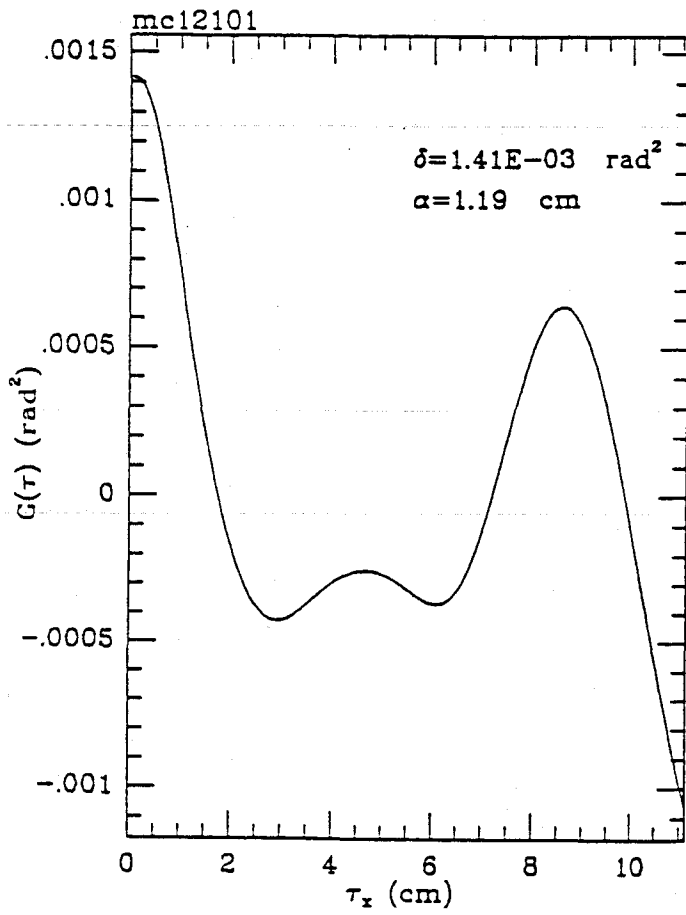
$\delta=1.41E-03$ rad^2
$\alpha=1.19$ cm

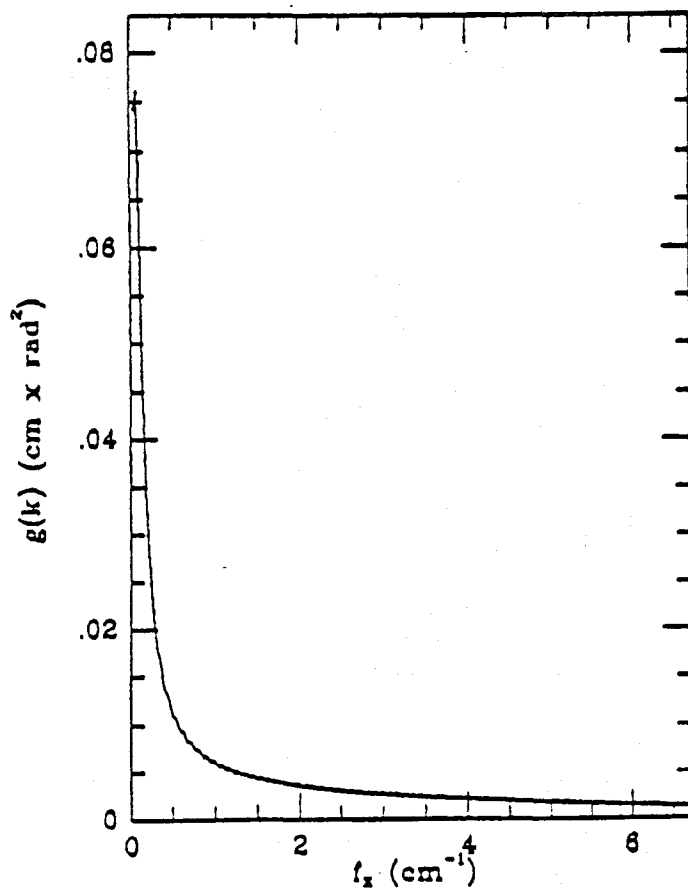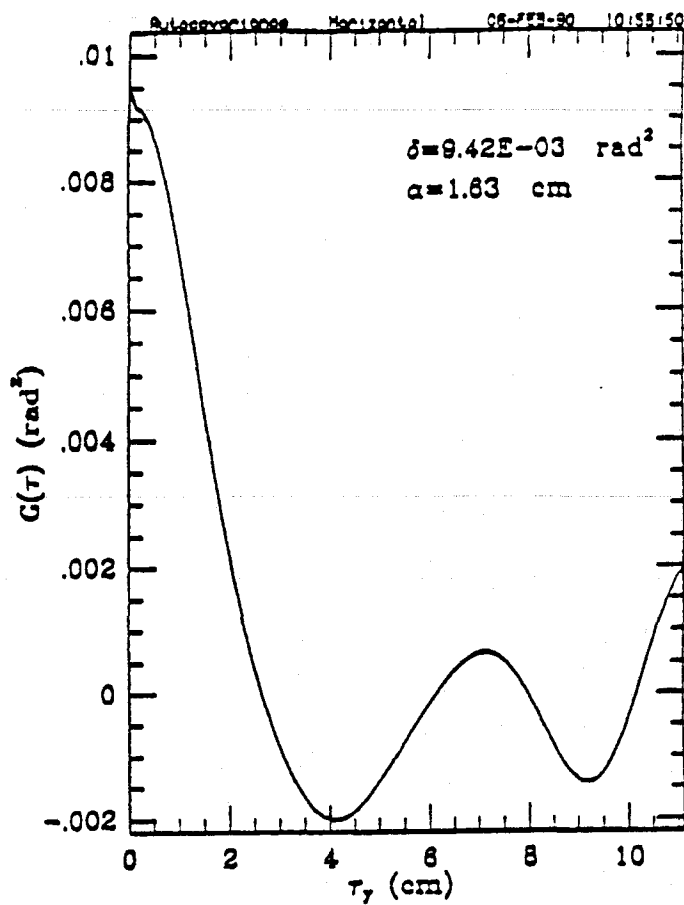$\delta=1.42E-03$ rad^2
$\alpha=0.67$ cm

Figure 29.   Autocovariance functions and their Fourier transforms calculated from a simulated phasefront.
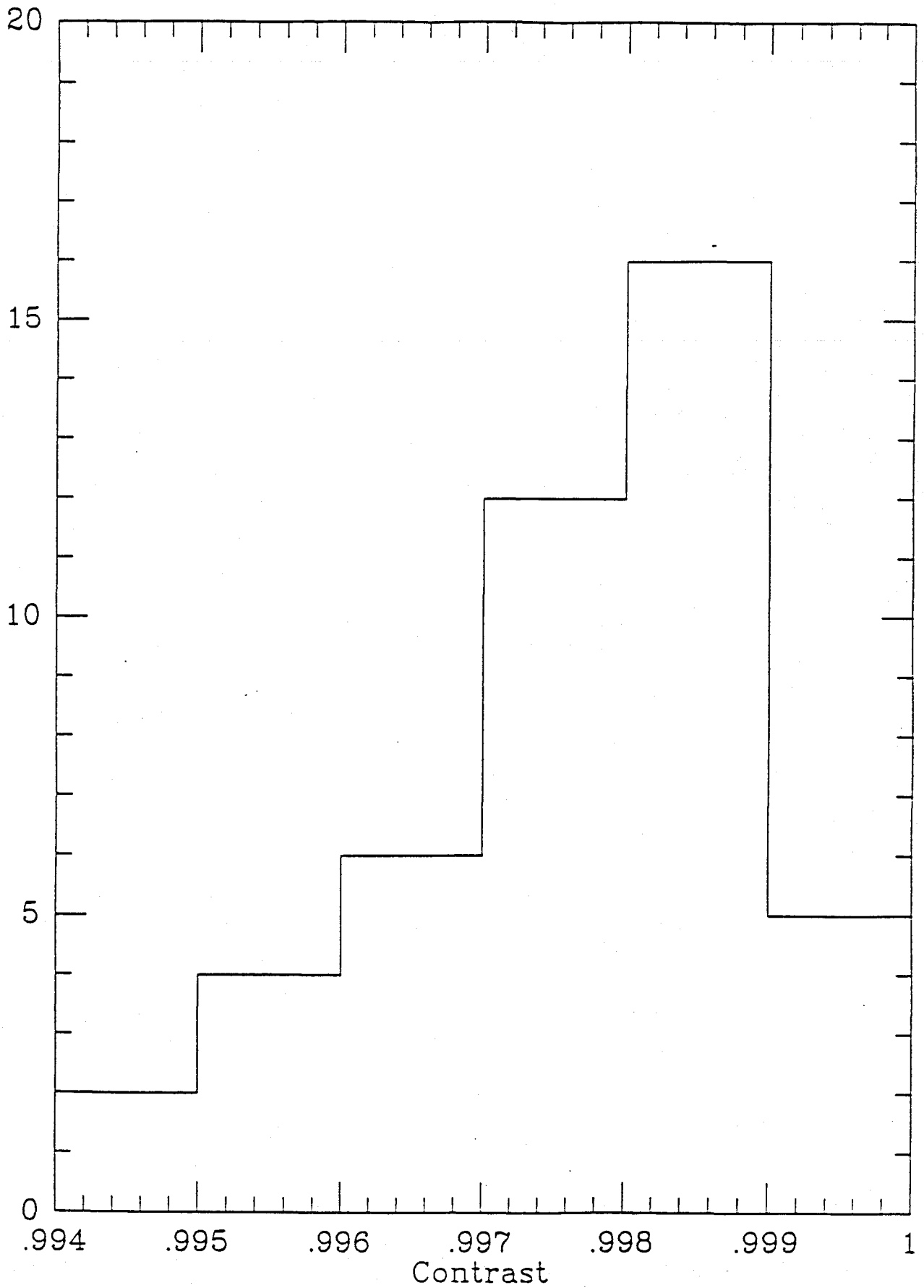
Figure 30.   Histogram of contrast values calculated for possible pairs
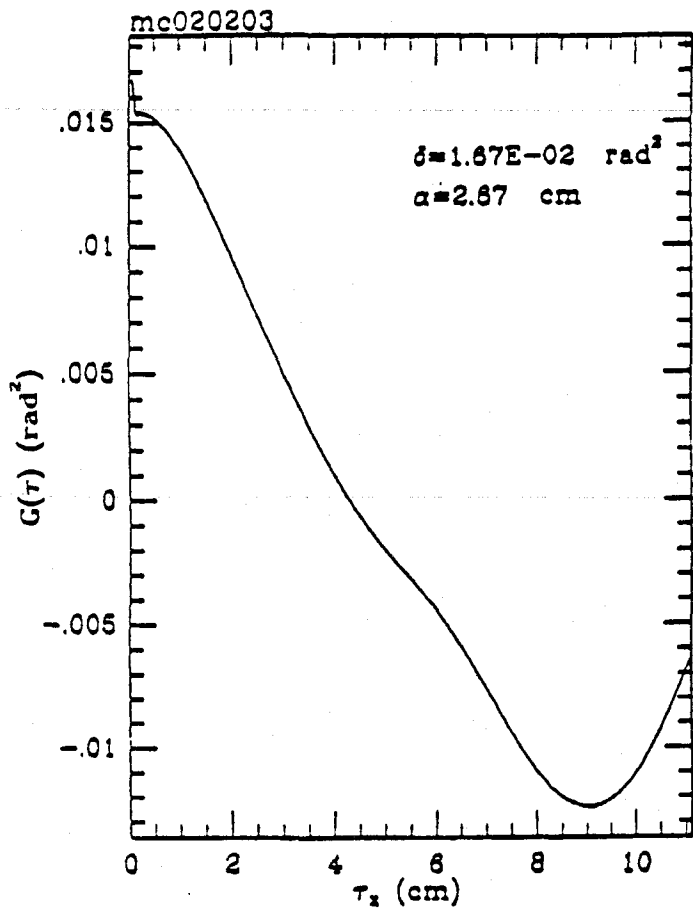of ten similar simulated mirrors.
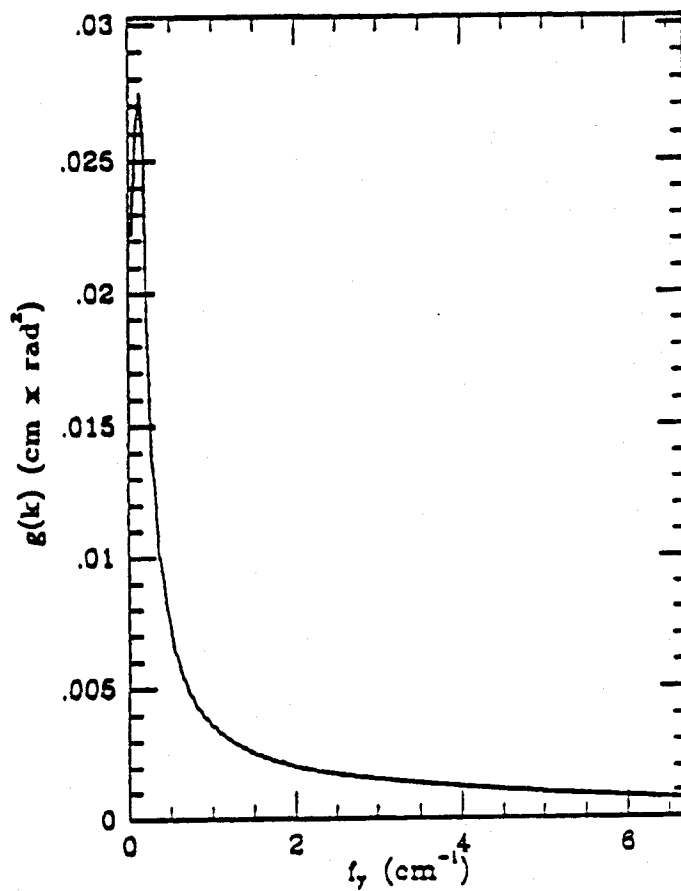
Figure 29.　Autocovariance functions and their Fourier transforms calculated from a simulated phasefront.
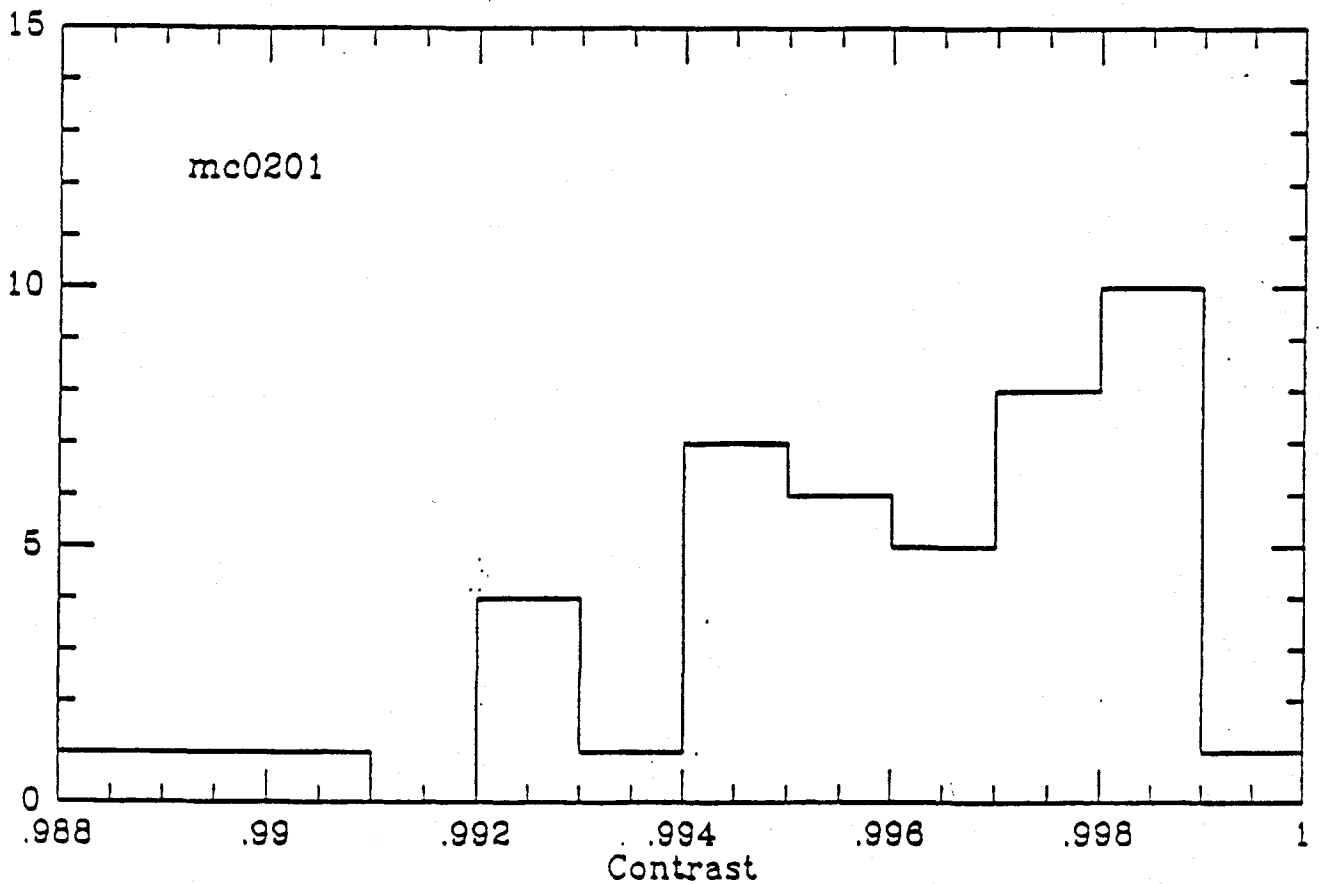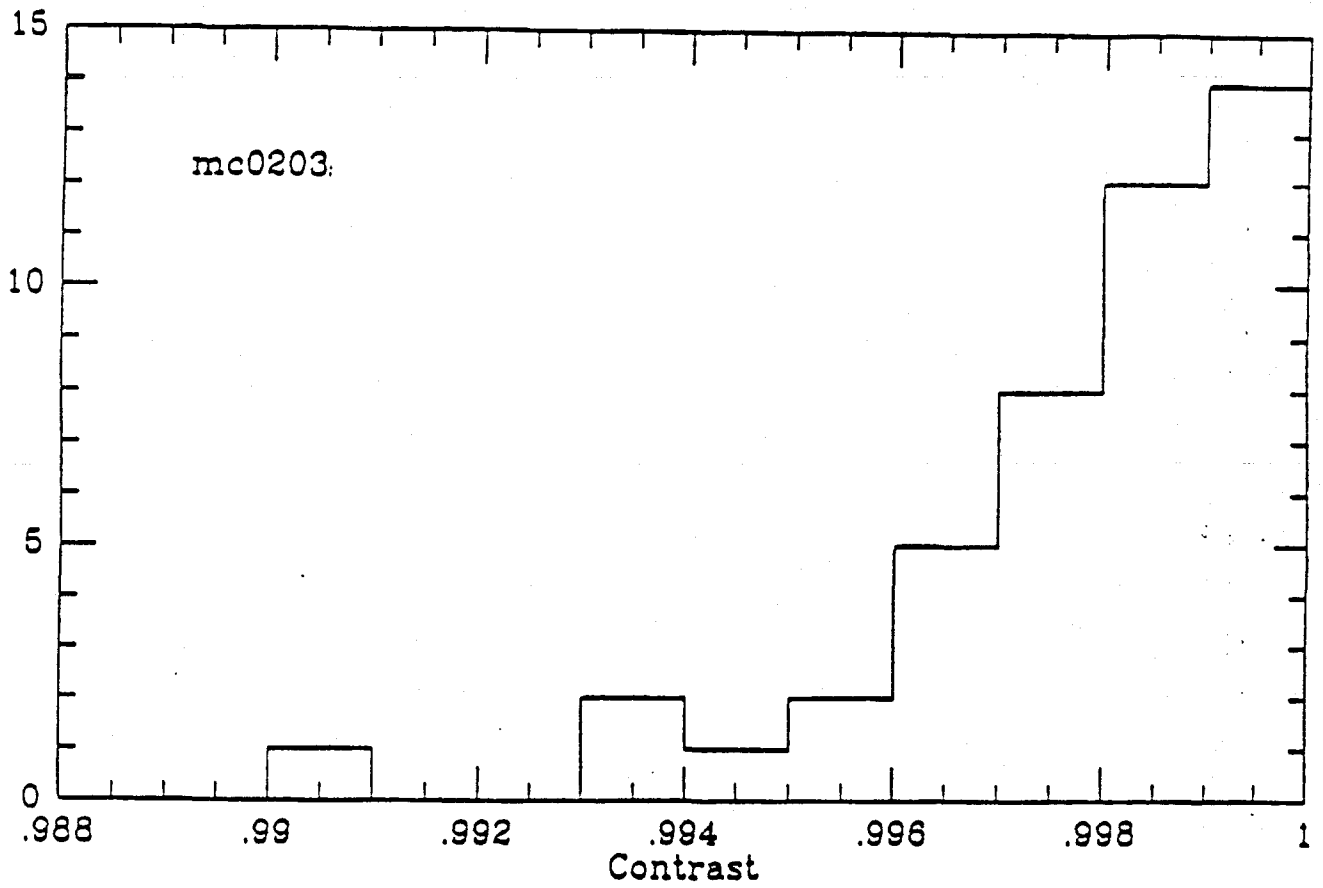
Figure 30. Histograms of contrast values calculated from Monte Carlo simulation of LIGO mirrors. Upper histogram is for inhomogeneities scaling with square root of thickness, lower blank for linear scalir